The ISLAS2020 field campaign: Studying the near-surface exchange process of stable water isotopes during the arctic wintertime

Andrew W. Seidl[1,2], Aina Johannessen[1,2], Alena Dekhtyareva[1,2], Jannis M. Huss[3,4], Marius O. Jonassen[1,5], Alexander Schulz[6], Ove Hermansen[7], Christoph K. Thomas[3,4], and Harald Sodemann[1,2]

[1]Geophysical Institute, University of Bergen, Bergen, Norway
[2]Bjerknes Centre for Climate Research, Bergen, Norway
[3]Micrometeorology Group, University of Bayreuth, Bayreuth, Germany
[4]Bayreuth Center of Ecology and Environmental Research, BayCEER, University of Bayreuth, Bayreuth, Germany
[5]The University Centre in Svalbard, Longyearbyen, Norway
[6]Alfred Wegener Institute, Helmholtz Centre for Polar and Marine Research, Potsdam, Germany
[7]NILU – Norwegian Institute for Air Research, Kjeller, Norway

Correspondence: Andrew W. Seidl (andrew.seidl@uib.no)

Abstract. The ISLAS2020 field campaign during February and March 2020 set out to obtain a unique dataset describing the Arctic water cycle using stable water isotope (SWI) observations. Our observation strategy focused on measuring evaporation, deposition, and precipitation, all of which are commonly sub-grid scale processes in numerical weather and climate models. Uncertain parameterizations for these processes can lead to compensating errors, which can go unnoticed; however, evaporation and precipitation can also be investigated with SWIs, as they are an integrated tracer for processes that atmospheric moisture has undergone. The campaign can be divided into two efforts: a localised field experiment in Ny-Ålesund focused on evaporation and deposition, and a larger precipitation collection network distributed around the Nordic Seas.

The Ny-Ålesund field experiment lasted three weeks, from 23 February to 15 March 2020, with temperatures reaching below -30 °C. During these weeks, we obtained near-surface, high-resolution (approx. 20 cm) SWI profiles at two deployment sites. Using a newly developed profiling system, we measured SWI gradients in the lowermost 5 and 2 m over fjord water and snow-covered tundra, respectively. These profiles are complemented by fiber-optic distributed sensing (FODS) columns and ambient conditions from nearby meteorological stations. The FODS columns supply continuous, high-resolution (2 cm or finer) temperature profiles above both locations, whereas the meteorological stations provide information on wind speed and direction. We also made a short deployment to the Zeppelin mountain observatory (472 m a.s.l) for measurements of the isotopic signal in the free-troposphere. Additionally, numerous water samples from the snowpack in and around Ny-Ålesund were taken, in addition to daily fjord water samples from Kongsfjorden. These samples provide the context for the surface conditions under which profiles were collected. Isotopic connections on the synoptic scale are achieved by linking Ny-Ålesund observations with precipitation sampling at locations across the European Arctic, namely Longyearbyen, Tromsø, Andenes, Ålesund, and Bergen. The resulting dataset provides comprehensive insight into the Arctic hydrological cycle and can facilitate the study of phase change processes and transport of water vapour into and out of the Svalbard region. Datasets from the field

campaign are publicly available at the PANGAEA data repository (doi.pangaea.de/10.1594/PANGAEA.971241, Seidl et al., 2024).

1 Introduction

The lowermost atmosphere near the marginal ice zone is characterized by large contrasts in temperature and moisture between ice-covered and ice-free areas. In this environment, water vapour undergoes numerous phase changes, for example when evaporating from relatively warm ocean waters into overlying cold air, subsequent formation of clouds, precipitation, and the condensation of water vapour from the atmosphere onto ice and snow. Adequately representing processes from such an extreme environment in numerical models remains highly challenging (e.g. Solomon et al., 2023). Therefore, the availability of suitable measurement data from these regions is key for model verification and development (Valkonen et al., 2020).

Being a natural integrating tracer for phase changes, measurements of the stable water isotope composition in water vapour and condensed water can provide additional information when trying to understand these processes. The composition can be quantified using the δ notation (Craig, 1961) for a particular isotope, i, as expressed in Eq. 1.

$$\delta i = \left(\frac{{}^{i}R_{samp}}{{}^{i}R_{stnd}} - 1 \right) * 1000 \quad ‰ \tag{1}$$

where ${}^{i}R_{samp}$ is the ratio of the heavy (i) to light isotopologue in the measured sample, ${}^{i}R_{stnd}$ is the same in a known reference standard, and δi is given in units of ‰ (parts per thousand, or permil). By studying how δ values change throughout the atmospheric water cycle, we gain knowledge on processes occurring during airmass transformation, for example the transformation from dry, polar to sub-arctic, moist airmasses, and vice versa (Thurnherr et al., 2021). Several regional models (e.g. Pfahl et al., 2012) and Earth system models (e.g. Brady et al., 2019) have been equipped with water vapour isotope physics. However, high-resolution in-situ measurements of water isotope composition during both condensation and evaporation in Arctic conditions remain severely lacking. Furthermore, coordinated measurement efforts enabling analysis of the isotopic imprint of airmass transformation as it is transported southward from the High Arctic to mainland Norway over the open waters of the Norwegian Sea are scarce. Such observational data are highly needed to test and evaluate different phase change processes in isotope-enabled models.

As water undergoes evaporation, vapour pressure differences amongst the various molecules of stable water result in the vapour being relatively depleted in the more massive isotopes compared to the liquid water. When this evaporation occurs under non-equilibrium conditions, characterized by surface gradients in wind, temperature and water vapour mixing ratio, the ratio of HDO to $H_2^{18}O$ in the vapour is larger than compared to equilibrium conditions. This relationship is encoded in the deuterium excess (d-excess) parameter, defined as d-excess $= \delta D - 8 * \delta^{18}O$ (Dansgaard, 1964), and it quantifies the effects of non-equilibrium fractionation, specifically kinetic fractionation. Foundational work has established a theoretical model to predict the water isotopic flux during evaporation in Arctic conditions (Craig and Gordon, 1965), while previous laboratory studies (Cappa, 2003; Barkan and Luz, 2007; Jouzel and Merlivat, 1984; Ellehoj et al., 2013) have investigated the impact that cold and dry conditions would have on the d-excess. Under these non-equilibrium conditions, the resulting d-excess of vapour

evaporated in the Arctic should have a positive signature. However, several long-range transport studies (Klein et al., 2015; Kopec et al., 2016) have associated a negative d-excess signature to moisture from the Arctic. Other recent studies underscore that both positive and negative atmospheric d-excess signatures may be found in polar regions (Thurnherr et al., 2021; Brunello et al., 2023), with a recent shipbourne study finding prominent complexity in the spatial pattern of stable water isotopes in the Arctic (Klein et al., 2024). A more nuanced view of the Arctic d-excess signal may thus be needed, one built considering drivers that allow for both positive and negative d-excess to exist in the Arctic.

The isotopic composition of the atmospheric vapour, including the d-excess, has been shown to be impacted by isotopic exchange between atmosphere and Arctic surfaces, for both oceanic (Thurnherr and Aemisegger, 2022; Brunello et al., 2024) and ice surfaces (Wahl et al., 2024; Casado et al., 2021). The imprint on the vapour depends on both the strength of the surface flux, as well as the direction of net exchange. Near the ice edge, and near leads in sea ice, relatively warm open water comes into contact with the atmosphere above, and establishes neutral to unstable stratification in the surface layer above the water. This establishes a corresponding positive (upwards) flux of sensible and latent heat. These positive fluxes are especially intense during marine Cold Air Outbreaks (CAOs; Papritz and Pfahl (2016); Kirbus et al. (2024)), where freeze-dried polar airmasses are transported southward over the ice edge and onto open water, resulting in a positive d-excess signature. Conversely, in the Arctic wintertime, stable stratification frequently prevails in the surface layer over snow and ice-covered surfaces, which can lead to hoar deposition as a result of a negative (downwards) fluxes of sensible and latent heat, which could in contrast create a negative d-excess in the remaining water vapour. In the marginal ice zone (MIZ), such acutely opposed surface fluxes could occur virtually simultaneously within a very short distance.

In such heterogenous terrain, highly detailed in-situ measurements over different surface conditions can help reconcile the different perspectives provided by existing laboratory, theoretical, and field studies on the kinetic isotope fractionation during phase change in the Arctic. For example, highly-resolved vertical profile measurements of the isotope composition and the thermodynamic environment in a natural environment can bridge the gap between the idealised context of laboratory studies (Cappa, 2003; Ellehoj et al., 2013) with measurements from a fixed-height on the order of meters above the surface (Leroy-Dos Santos et al., 2020; Brunello et al., 2023). As laboratory work often focuses on small-scale processes occurring on short time scales while fixed-height field installations measure a more integrative signal over longer times, measurements with high resolution in space and time spanning the gap between these two types of observations gives valuable context to both. And by focusing on surface-atmosphere exchange in the Arctic, one thereby gains access to both the source signature of Arctic moisture, as well as essential information for subsequent transformation of this signal when transported southward away from the Arctic.

Here we present a comprehensive dataset of the water isotope composition of atmospheric water vapour, surface snow, sea water, and precipitation from the European Arctic and downstream locations in Norway, obtained during the ISLAS2020 field campaign in Feb-Mar 2020. Using a near-surface profiling system (Seidl et al., 2023), we have performed numerous SWI profiles of the surface layer in Ny-Ålesund, Svalbard. Our deployments over snow-covered tundra and coastal fjord water probed the lowermost 2 and 5 m above the surface, respectively. Alongside these profiles, surface samples of snow and water were also collected. At both locations, in cooperation with NYTEFOX (NY-Ålesund TurbulencE Fiber Optic eXperiment)

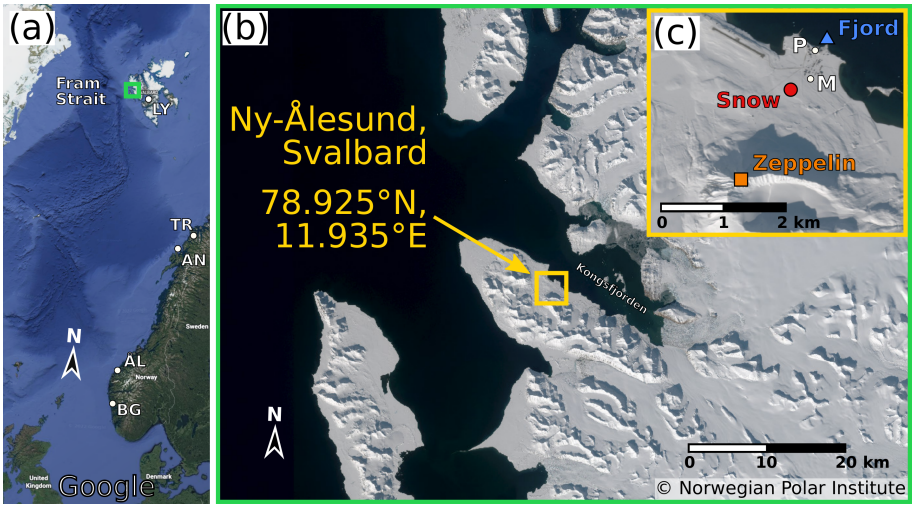

Figure 1. The study region. (a) Experiment area around Ny-Ålesund (green square) alongside additional precipitation collection sites (LY: Longyearbyen, TR: Tromsø, AN: Andenes, ÅL: Ålesund, BG: Bergen) (© Google Earth 2022). (b) The western coast of Spitsbergen and Kongsfjorden, with the settlement of Ny-Ålesund along the southern shore (yellow square). (c) The three deployment sites (Snow, Fjord, and Zeppelin) in relation to Ny-Ålesund. Also shown is the location of the precipitation collector (P) and the 10 m meteorological mast (M). (b,c: © Norwegian Polar Institute, http://toposvalbard.npolar.no).

(Zeller et al., 2021), we obtained collocated high-resolution vertical temperature measurements from fiber-optic distributed sensing (FODS) instrumentation. With the measurement strategy employed, the FODS methods provided temperature profiles with at least 2 cm vertical resolution, down to 0.25 cm resolution. The isotopic state of the free-troposphere was obtained with a short deployment to the nearby Zeppelin mountain observatory. Throughout the campaign, we collected discrete precipitation samples in both Ny-Ålesund and Longyearbyen in Svalbard, and at four stations along the coast of the Norwegian mainland, providing upstream and downstream context for the Arctic water isotope signatures. Our dataset thus in combination provides unprecedented water isotope information from the wintertime Arctic for use in both process studies and model development.

2 Campaign locations and weather conditions

The ISLAS2020 field campaign took place over a 35 day period from 20 February to 25 March 2020, with the localised experiment site being in the scientific settlement of Ny-Ålesund (78.925°N, 11.935°E), Svalbard from 23 February to 15 March. The campaign was organized into several measurement deployments at the experimental site, and precipitation sampling across a network of downstream southerly locations (Figure 1a). We first provide an overview of the entire campaign network, including typical environmental conditions of the experiment site. This is followed by a timeline of the synoptic conditions during the campaign period.

2.1 Campaign network

The main location of the ISLAS2020 campaign was the scientific settlement of Ny-Ålesund, Svalbard, Norway, hosting the localised field experiments. Ny-Ålesund is located on the southern shore of Kongsfjorden, on the western coast of Spitsbergen, Svalbard's largest island (Figure 1a,b). Given its close proximity to the Fram Strait, the location is well-suited to measure in conditions that can occur within the MIZ, for example during CAOs, for which the Fram Strait is a wintertime hotspot (Papritz et al., 2019). Long-term measurement data from Ny-Ålesund from multiple international atmospheric research efforts thereby provide context to the observations performed in spring 2020.

A $10\,\mathrm{m}$ meteorological mast has been in operation near the southern edge of the settlement by the Alfred Wegener Institute (AWI) since 1993 (Maturilli et al., 2013b) (Figure 1c, "M"). The 1999-2019 February-March climatology has a median $2\,\mathrm{m}$ air temperature of -10.8 $^\circ\mathrm{C}$, with a median $2\,\mathrm{m}$ dewpoint temperature of -15.9 $^\circ\mathrm{C}$ (Maturilli et al., 2013a; Maturilli, 2020). Despite the average sub-zero temperatures, since 2012 the fjord typically has less than $50\,\%$ fast-ice coverage during February and March, with a negative trend of about -4 $\%/\mathrm{year}$ since 2003 (Gerland et al., 2020). The ice is also typically more concentrated towards the northern shore of the fjord. The topography around the fjord influences the wind speeds observed at $10\,\mathrm{m}$ above ground, with the main flow direction coming from the SE, parallel with the fjord axis (Maturilli et al., 2013a; Maturilli, 2020) (Figure 1b). Almost perpendicular to the main fjord axis is the second most prevalent wind direction, coming from the WSW (Maturilli et al., 2013a; Maturilli, 2020), with mostly slow winds outflowing from the nearby Brøgger glaciers (Schulz, 2017). Less frequently, higher wind speeds are associated with winds from the WNW that enter from Fram Strait along the main fjord axis.

In addition to the measurement site in Ny-Ålesund, a network for collection of discrete precipitation samples was operated at a total of six locations (Ny-Ålesund, Longyearbyen (LY), Tromsø (TR), Andenes (AN), Ålesund (AL), and Bergen (BG), Figure 1a). Longyearbyen is also in Svalbard and approximately $110\,\mathrm{km}$ away from Ny-Ålesund. Tromsø, Andenes, Ålesund, and Bergen are located across the Norwegian sea, on the Norwegian mainland, at a distance of $1050\,\mathrm{km}$, $1100\,\mathrm{km}$, $1850\,\mathrm{km}$, and $2100\,\mathrm{km}$, respectively.

2.2 Overview of synoptic conditions during the campaign

The campaign period was dominated by northerly flow, with some interspersed periods of warm air advection. During the first ten days of the Ny-Ålesund experiment (23 February to 3 March), the large-scale circulation brought cold and dry airmasses from the interior of the Arctic towards Ny-Ålesund from the north. The cold air overlying the warm, open ocean established distinct marine CAO conditions (Figure 2a). The strength of a CAO is quantified by the CAO index (CAOi) which is the difference between the potential temperature at the sea surface and $850\,\mathrm{hPa}$. These CAO events (CAO1 and CAO2, Figure 2a) proceeded south, reaching as far south as Ålesund. Thereafter, around 3 March, a low pressure system approaching from the south reversed the flow at Ny-Ålesund. This flow reversal was associated with warmer, more moist conditions with total column water vapour (TCWV) up to $4.7\,\mathrm{kg\,m^{-2}}$ (Figure 2a,b). Such a weather pattern into the Arctic can be described as a Warm Air Intrusion (WAI, Dunn and Grice (1975)). The WAI lasted until about 8 March; after which, CAO conditions returned until the

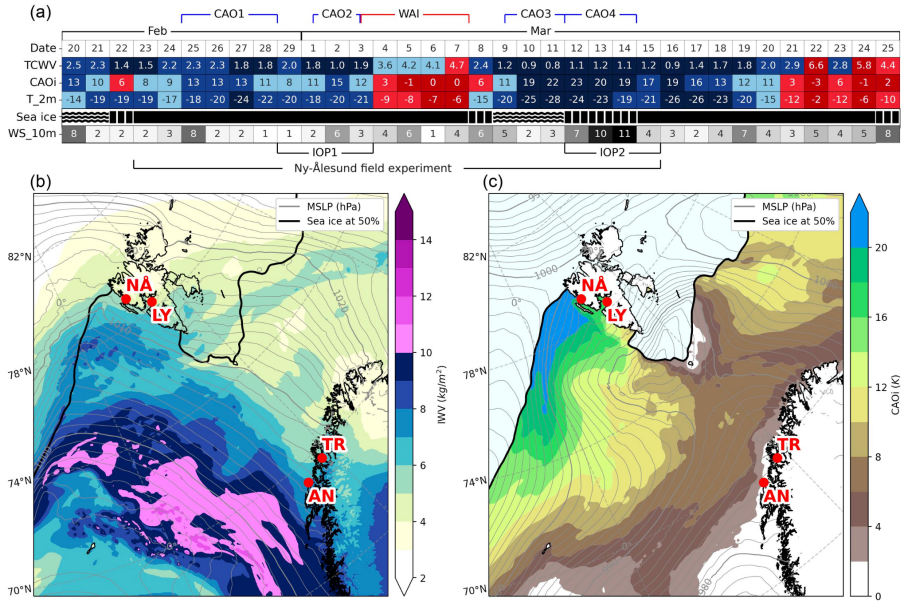

Figure 2. Synoptic conditions during the ISLAS2020 field campaign. (a) Overview table of conditions in Ny-Ålesund during the campaign. Total column water vapour (TCWV) ($\mathrm{kg\,m^{-2}}$) and Cold air outbreak index (CAOi) (K) from ERA5. 2 m Temperature and 10 m wind from AWI weather station. Sea-ice observation at the new pier. (b) Integrated water vapour (IWV) (shading) alongside sea level pressure (MSLP) (grey contours) for 5 March 2020 00UTC from AROME-Arctic. (c) The CAOi (shading) for 11 March 2020 12UTC from AROME-Arctic. Thick black line denotes sea ice concentration at 50 %.

end of the Ny-Ålesund experiment (Figure 2a). These CAO (CAO3 and CAO4) periods were stronger than their predecessors (CAOi > 20 K, Figure 2a,c), with CAO4 coming with higher wind speeds. During these periods, the entire sampling network encountered CAO conditions. These CAOs were of record strength for the Fram Strait for that time of year (Dahlke et al., 2022).

Counter to the typical trend, the low temperatures during (and preceding) CAO1 also brought abnormally extensive sea-ice coverage, though at the end of the WAI on 8 March, the sea ice experienced extensive break up and exposed open fjord water at the northern edge of the settlement (Figure 2a, "Sea Ice").

Two Intense Observing Periods (IOPs) were initiated during the experiment time period, involving higher frequency sample collection across the sampling network, where possible. IOP1 occurred between CAO1 and the WAI, entirely including CAO2, from 29 February to 3 March. IOP2 began on 12 March and ended on 15 March, coinciding with the onset and conclusion of CAO4.

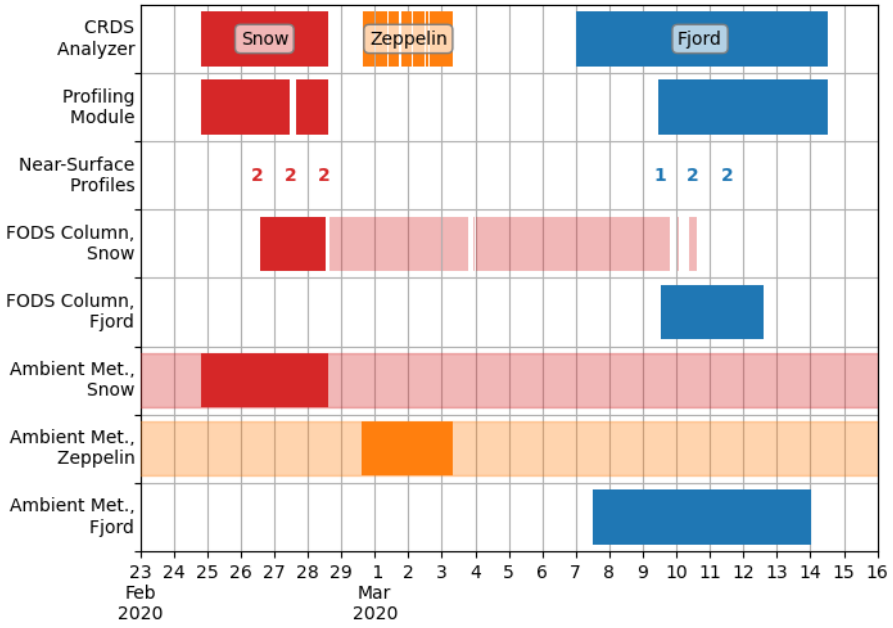

Figure 3. Timeline of instruments and deployment locations during ISLAS2020 during the field experiment in Ny-Ålesund, Norway, with colours indicating individual deployments. Dark coloured bars denote timeframes included in the ISLAS2020 dataset files, while faded bars indicate instrument uptime beyond the scope of the ISLAS2020 dataset. Number of discrete events given for the calendar day (UTC).

3 Campaign activities

We now present details of campaign activities at the specific deployment sites in Ny-Ålesund as well as the locations across the sampling network. Overviews of instrument uptimes at the Ny-Ålesund experiment and collections from the sampling network can be found in Figures 3 and Figure 4, respectively.

3.1 Ny-Ålesund experiment operations

In order to quantify the isotopic structure of water vapour in the near-surface, we conducted detailed profiling operations of the near-surface atmosphere during different weather conditions at two deployment locations in Ny-Ålesund.

First, profile measurements were performed over the snow-covered tundra in the vicinity of a fiber-optic distributed sensing (FODS) measurement network set up within the NYTEFOX experiment (Zeller et al., 2021), about 300 m south of the settlement (Figure 1c, site "Snow" at 78.92117°N, 11.91361°E, 27 m a.s.l.). Thereafter, profile measurements were obtained from a concrete pier over the partly ice-covered water of Kongsfjorden near the Marine Laboratory in the northern part of the settlement (Figure 1c, site "Fjord", 78.92873°N,11.93552°E). These profiling operations took place, at least in some part, during two of the CAO periods (CAO1 and CAO3). During the profiling deployments, the ambient temperature was almost 10 K

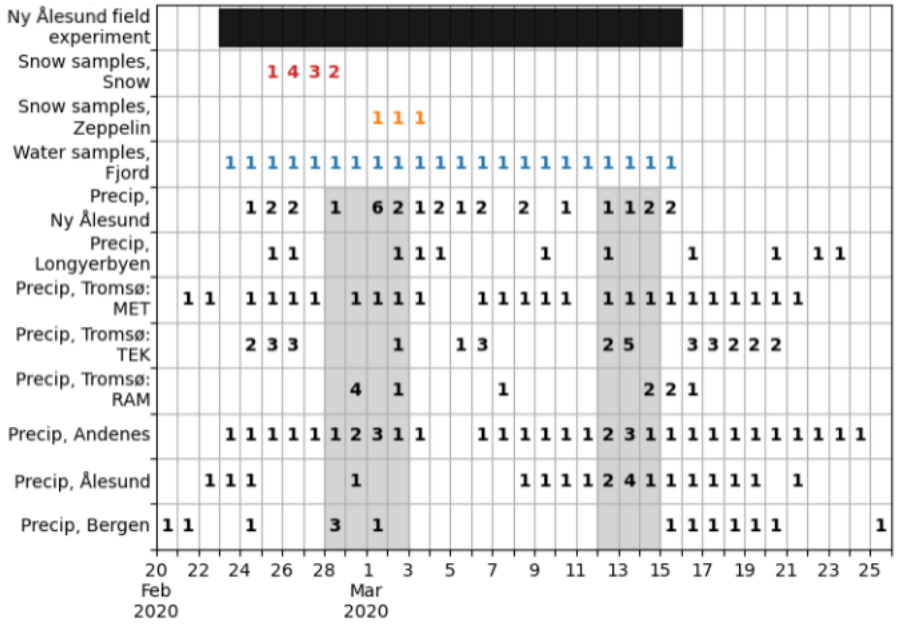

Figure 4. Sampling timeline for ISLAS2020. Number of discrete events given for the UTC calendar day, with collection time used to determine day. For reference, the overall duration of the field experiment in Ny-Ålesund is indicated by the black bar (time scale of Figure 3). Grey shading indicates the two IOP periods for precipitation sampling.

colder (-19.7 °C) than the climatological median, and had a median dewpoint of -24.3 °C (Maturilli et al., 2013a; Maturilli, 2020).

Between both profiling deployments, isotopic measurements of ambient vapour were performed at the Zeppelin Observatory (hereafter referred to as "Zeppelin") on Zeppelin Mountain at 472 m a.s.l and approximately 2 km to the SW of Ny-Ålesund (Figure 1c). These observations provided insight into the isotope composition of the free troposphere, giving context to the near-surface profiles measured at Ny-Ålesund.

Though the exact configuration varied between the deployment sites, both sites required common components of instrumentation (Figure 5): (1) a cavity ring-down spectrometer (CRDS) inside a field deployment system attached to an articulating profiling arm (Seidl et al., 2023) (Figure 5, **ic**); (2) a nearby fiber-optic distributed temperature sensing column (Figure 5, **fc**); and (3) a nearby meteorological station providing information on the ambient conditions (Figure 5, **ec** and **ws**). The instrument setup at Zeppelin involved only a CRDS analyzer measuring near to the meteorological station of the observatory.

We now present the details of the deployed installation at the three locations Snow site, Fjord site and Zeppelin. The calibration and post-processing protocols for the CRDS isotopic measurements are described jointly for all sites in Sec. 4.1.1.

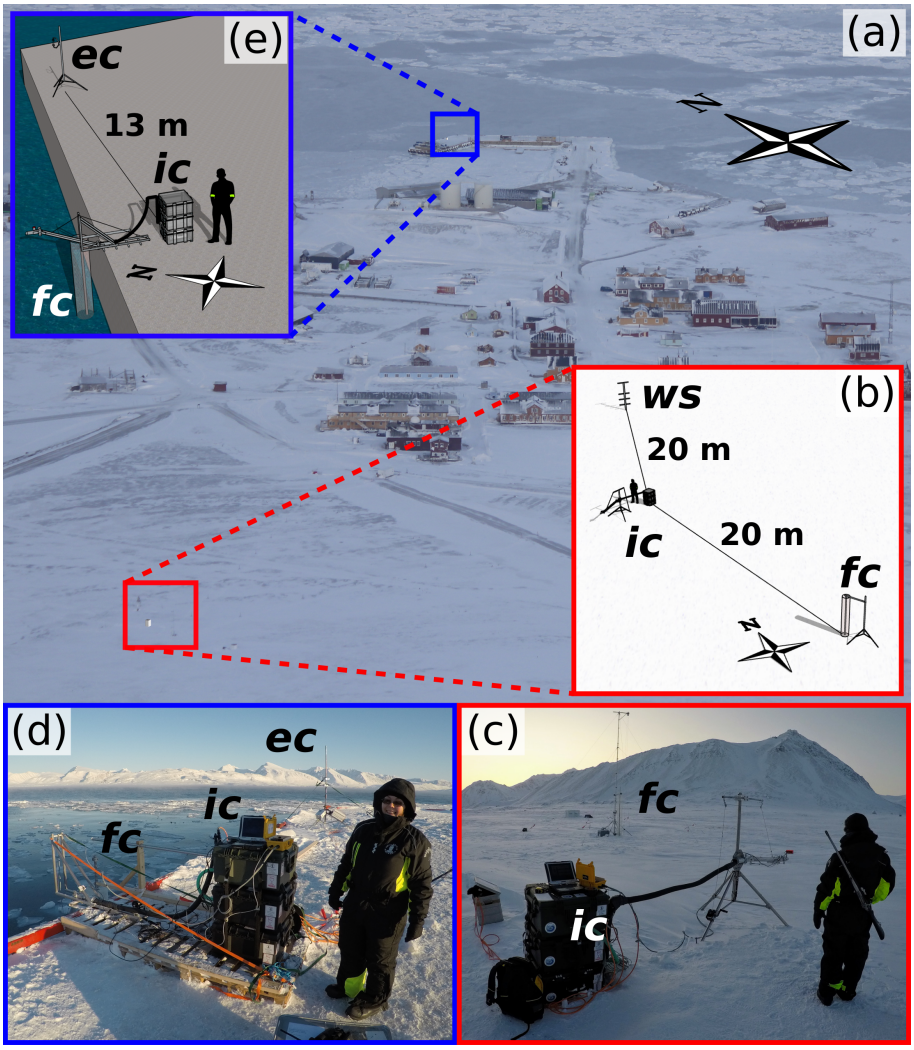

Figure 5. An overview of the two profiling deployment sites. (a) Ny-Ålesund as seen from Zeppelin Observatory (From 1 March 2020), including positions of Snow (red square) and Fjord (blue square) deployment sites. (b) Site schematic of the Snow site, and (c) Field photo of the Snow site, taken facing approximately south. Snow instrument abbreviations: **ic**: ICE-CUBE profiling system; **fc**: Fiber-optic distributed temperature sensing column; **ws**: automatic weather station operated by the Alfred Wegener Institute. Note that **ws** is behind the picture field of view. (d) Field photo of the Fjord site, facing northwest, and (e) Site schematic of the Fjord site. Fjord instrument abbreviations: **ic**: ICE-CUBE system; **fc**: Fiber-optic distributed temperature sensing column; **ec**: temporary eddy-covariance station.

Table 1. Instruments deployed/present at the Snow site from 24 Feb to 28 Feb, with corresponding measurement parameters, units, and measurement height range. Heights are given relative to local ground level (approximately 27 m a.s.l., EPSG:4258).

Instrument	Parameter	Unit	Height (m)
ISE-CUBEs	δ^{18}O, δD	‰	0.04 to 2.02
	Specific humidity (at inlet)	$\mathrm{g\,kg^{-1}}$	0.04 to 2.02
	Air temperature (at inlet)	K	0.04 to 2.02
	Inlet height	m	0.04 to 2.02
Automatic weather station	Air temperature	K	2.1, 1.5, 1.0, 0.5
	Wind speed and direction	$\mathrm{m\,s^{-1}}$	2.1, 1.5, 1.0, 0.5
FODS column	Temperature	K	-0.25 to 2.25
Snowpack samples	Surface and hoar	-	-0.01 and -0.002

3.2 Snow deployment site setup and operations

We acquired detailed near-surface profiles of water vapour isotope composition using the articulating sampling arm of the so-called ISE-CUBE profiling system (Seidl et al., 2023), supplemented with additional instrumentation (Table 1). A Picarro L2130-i CRDS analyzer (Picarro Inc., Sunnyvale, USA; Ser#: HIDS2254) and its necessary accessories were encased in a field deployment system consisting of three ventilated, weatherproof plastic cases (Seidl et al., 2023). The analyzer is configured to measure at 4 Hz with a flow rate of around 0.15 $\mathrm{L\,min^{-1}}$ through the measurement cavity. The sample inlet of the analyzer is connected via approximately 4 m of heated, stainless steel tubing to an articulating arm mounted to a tripod (Figure 5b,c; **ic**); this tubing is flushed at a a rate of approximately 9 $\mathrm{L\,min^{-1}}$. The head height of this arm can be adjusted between 4 and approximately 200 cm above the surface, allowing for vapor sampling at any height in this range. Attached to the head are height and temperature sensors, logging at 1 Hz to a microcontroller (Arduino Uno). The system allows for the acquisition of vertical profiles with a temporal resolution of at least 4 min (Seidl et al., 2023). The measurements over the snow were conducted from 24 February 20:00UTC to 28 February 14:15UTC, and yielded six profiles with between 110 to 248 data points, corresponding to 55 to 124 min (Figure 3). A detailed example of such data is given in Sec. 5.1).

Very high-resolution profiles of the air temperature were acquired approximately 20 m to the southeast of the ISE-CUBEs by a 2.5 m tall FODS column as part of the NYTEFOX campaign (Figure 5b,c; **fc**). In brief, the FODS column consisted of a fiber-optic cable wrapped helically around a cylindrical glass-mesh frame (32 cm diameter). This glass-mesh was connected to an aluminium rod which was suspended from a support arm approximately 2.4 m up a single mast tower. The bottom of the column was buried in the underlying snowpack, yielding temperature measurements across the snow-air interface. The column was in (non-continuous) operation from 26 February 13:44UTC to 10 March 14:55UTC (Figure 3), providing data at 0.25 to 2 cm vertical and 9 s temporal resolution with a typical precision of 0.28 °C. More details can be found in Zeller et al. (2021), with the corresponding dataset available at Huss et al. (2021).

Table 2. Discrete water samples taken for stable water isotope analysis during the field experiment in Ny-Ålesund.

Coverage Start	Coverage End	Sample Type	Location	Count
2020-02-25	2020-02-28	Surface snow	Snow site	4
2020-02-25	2020-02-28	Hoar (frost flowers)	Snow site	3
2020-02-26	2020-02-26	Snow pit	Gruvebadet	3
2020-02-23	2020-03-15	Fjord water	Fjord site	22
2020-03-01	2020-03-03	Surface snow	Zeppelin	3
2020-02-24	2020-03-15	Snow (precipitation)	Marine Laboratory	29

Approximately 20 m north of the ISE-CUBE installation site, an automatic weather station monitored ambient conditions (Figure 5b; **ws**). Operated by the Alfred Wegener Institute since 2010 (Jocher et al., 2012; Schulz, 2017), this station records temperature and wind conditions at four levels (0.5, 1.0, 1.5, and 2.1 m). Temperature sensors (2.1280.00.160, Adolf Thies GmbH & Co. KG) are housed in ventilated shields (1.1025.55.100, Adolf Thies GmbH & Co. KG). Wind conditions are monitored with propeller style wind anemometer/vane combinations (5106-5 at 0.5 1.0, 1.5 m and 5103-5 at 2.1 m; R. M. Young Company). The station also monitors infrared surface temperature (IR100, Campbell Scientific, Ltd.) which can be used to derive snow surface temperature. The station measures at 0.5 Hz and records to a CR3000 datalogger (Campbell Scientific, Ltd.).

In order to capture the isotopic evolution of the surface snow underlying our profile, we collected a daily sample of the uppermost layer of the surface snow from 25 to 28 February 2020 in an undisturbed section of snow approximately 3 to 5 m away from the profiling system. Surface snow samples were always taken in the afternoon, between 13:15 and 15:15UTC. Using a small pre-chilled plastic spoon, the uppermost 1 cm of a less than 50 cm^2 patch of snow was scraped off and filled into a plastic sample bag (58 mL Whirl-Pak, Nasco Sampling). These samples were then left to melt in the Marine Laboratory before being transferred to 1.5 mL glass vials (2-SVW Chromacol, Thermo Fisher Scientific Inc.) and immediately capped and stored until laboratory analysis (Sec. 4.4). A similar methodology was applied to the collection of hoar frost on the snow surface on 27 and 28 February, albeit scraping a larger area of only the uppermost 0.1 to 0.2 cm. In addition, snowpack samples were taken at 3 different layers in the nearby Gruvebadet site during the routine black carbon sampling. An overview of samples collected at the Snow site and surrounding area is given in Table 2 and Figure 4.

3.3 Fjord deployment site setup and operations

A second set of near-surface profiles of water vapour isotope composition was obtained at the Fjord site (Figure 1c). Fjord site measurements combined the ISE-CUBE profiling system for water vapour isotope composition, a FODS column for temperature profiles, and an eddy-covariance station for ambient meteorological parameters (Table 3). The analyzer measured again at 4 Hz with a flow rate of around 0.15 $\mathrm{L\,min^{-1}}$ through the measurement cavity. Measurement frequencies for the CRDS analyzer and profiling arm remained the same. However, due to the differing surface condition (sea ice and open water), some

Table 3. Instruments deployed at the Fjord site from 7 Mar to 15 Mar, with corresponding measurement parameters, units, and measurement height range. Heights are given relative to instantaneous (fjord) water level (EPSG:5829).

Instrument	Parameter	Unit	Height (m)
ISE-CUBEs	δ^{18}O, δD	‰	0.36 to 4.97
	Specific humidity (at inlet)	$\mathrm{g\,kg^{-1}}$	0.36 to 4.97
	Air temperature (at inlet)	K	0.36 to 4.97
	Inlet height	m	0.36 to 4.97
Eddy covariance station	Air temperature (sonic)	K	4.0 to 6.0 (2.0 above pier)
	Wind speed and direction	$\mathrm{m\,s^{-1}}$	4.0 to 6.0 (2.0 above pier)
	Air pressure	hPa	4.0 to 6.0 (2.0 above pier)
FODS column	Temperature	K	0.0 to 3.8
Fjord water samples	Surface	-	-0.3 to 0

modifications were required to the setup. A detailed example of measurement data from the Fjord site for 10 March is given in Sec. 5.1.

Since measurements were made from the pier wall over open water or sea ice, the ISE-CUBE system with its aluminium profiling arm was mounted in a tipping frame (Figure 5d,e; **ic**). This tipping steel frame allowed reaching an additional 1.5 m below the level of the concrete pier, substantially closer to the surface of the water (Seidl et al., 2023). Given the tidal variations at the site, this extension effectively allowed for profiles between just above 0 m to approximately 5 m above water level. In order to monitor the distance above the water in this downward orientation, the profiling head contained an additional front-facing ultrasonic sensor. Using this setup, a total of 5 profiles were performed on 3 different days. Profiling ranged from 0.36 to 4.74 m above the surface and lasted between 37 to 143 min. During the remaining measurement time at the Fjord site, the inlet head was kept at or above pier level (2.5 to 5.0 m above the water) to measure the near-surface water vapour isotope composition at fixed level. This procedure also minimized risk from sea-spray entering the system, especially during the high wind conditions on 13 and 14 March (Figure 2a).

The Fjord site FODS column was overall very similar to the Snow site column, with a diameter of 32 cm, a length of approximately 2.5 m, and with coil spacing increasing towards the upper end (see Thomas et al. (2022) for technical details). The Fjord column's central support rod was fixed to a wooden support arm at the NE edge of the ISE-CUBE wooden support platform. Then the whole column was suspended over the water, approximately 50 cm from the north face of the pier. Due to the tides, the distance between water level and column bottom fluctuated by approximately 1.5 m, including partial immersion of the column in the fjord water; this will be discussed in Sec. 4.3. The FODS column provided temperature measurements at a vertical resolution of 0.25 to 2 cm at 0.1 Hz with a typical precision of 0.28 °C. The column began operation on 9 March at

13:52UTC and provided observations until being crushed by drifting ice on 12 March at approximately 00:00UTC, whereafter data quality significantly degraded.

Ambient meteorological information at the Fjord site was acquired from an eddy-covariance station, located 13 m to the NE of the ISE-CUBE setup (Figure 5d, **ec**). A sonic anemometer (CSAT3, Campbell Scientific Ltd.), provided 3D wind information in addition to sonic temperature at a measurement height of 2.0 m above the pier deck. Alongside the sonic anemometer, we installed an open path water/CO_2 sensor (LI-7500, LI-COR, Inc), measuring ambient atmospheric pressure, water vapour concentration, and CO_2 concentration. The measurement volume of the water/CO_2 sensor was on the order of 20 cm away from the sonic anemometer measurement volume, with the water/CO_2 sensor tilted about 30° from vertical. Due to tidal variations and the height of the pier, this resulted in a measurement height of between 4.5 to 6.0 m above the water surface. Orientation of the anemometer towards 21° NNE (True) was such that the array axis was perpendicular to the predominant fjord-axis flow, leaving the typical flow direction unobstructed by the instrument and mast. The station logged the measurements from the sonic anemometer and the open path gas sensor at 20 Hz and recorded the incoming data stream to a CR5000 datalogger (Campbell Scientific, Ltd.). The installation was in place from 7 March 12:05UTC to 14 March 19:47UTC. However, heavy sea spray during the night from 13 to 14 March significantly reduced the quality of the ultrasonic measurements after 13 March 22:30UTC. Prior to this sea spray event, the sonic temperature was indistinguishable from both air temperature and virtual temperature at the given uncertainties, owing to the low humidities encountered. Therefore, the sonic temperature can be taken to be equivalent to air and virtual temperature. Additionally, a persistent instrument error only diagnosed after the conclusion of the field experiment, rendered the water vapour and CO_2 concentration measurements from the open path gas sensor of insufficient quality for use and therefore they will not be discussed further.

Throughout the entire field experiment, we collected daily fjord water samples in the vicinity of the pier. To this end, the uppermost 10 to 30 cm of the water column were retrieved with a clean and dry 10 L plastic bucket that was lowered on a rope into the water. Immediately after collection, we measured the temperature and salinity in the bucket with a handheld datalogger (Ponsel Odeon X, Aqualabo Group) and sensor (Ponsel C4E, Aqualabo Group) combination. Instrument failure on 11 Mar prevented further in-situ measurements after this time. As a result of the variable sea ice conditions, both the exact location and sampling depth varied to some extent throughout the campaign. Fjord water samples were collected in 1.5 mL GC screwcap vials and sealed with parafilm until later laboratory analysis of the water isotope composition at FARLAB (University of Bergen, Bergen, Norway). In total, 22 daily samples were collected from 23 Feb to 15 Mar (Table 2 and Figure 4).

3.4 Zeppelin deployment site setup and operations

The deployment at the Zeppelin site consisted of the CRDS analyzer only, with corresponding calibration equipment, surface snow sampling, and additional measurement parameters acquired from permanent installation (Table 4). While located at the observatory, the analyzer sampling can be divided into three distinct periods, based on the permanent or temporary inlet line used (Table 5). From 15:30UTC on 29 February to 14:40UTC on 1 March (ZEP1 period), the analyzer was connected to Zeppelin's main heated inlet line (21 m, 30 °C, 10 L min^{-1}) via a 10 m long section of existing ¼-inch plastic tubing already installed at the observatory. The plastic tubing was a combination of Bev-A-Line (about 4 m) and PTFE tubing (about 6 m).

Table 4. Instruments deployed/present at the Zeppelin site from 29 February to 3 March, with corresponding measurement parameters, units, and measurement height range. Heights are given relative to sea level (EPSG:4258).

Instrument	Parameter	Unit	Height (m)
CRDS analyzer	δ^{18}O, δD	‰	475 or 490
	Specific humidity (at inlet)	$\mathrm{g\,kg^{-1}}$	475 or 490
Automatic weather station (Zeppelin observatory)	Air temperature	K	490
	Air pressure	hPa	490
	Specific humidity	$\mathrm{g\,kg^{-1}}$	490
	Wind speed and direction	$\mathrm{m\,s^{-1}}$	490

Table 5. Periods of the deployment at the Zeppelin site from 29 February to 3 March.

Period name	Start time (UTC)	End time (UTC)	Inlet details	Total length (m)
ZEP1	29 Feb 15:30	1 Mar 14:40	Main inlet ($10\,\mathrm{L\,min^{-1}}$) and 10 m plastic (< $0.1\,\mathrm{L\,min^{-1}}$)	31
ZEP2	1 Mar 15:25	2 Mar 14:30	4 m Stainless steel/PTFE, (half heated) ($9\,\mathrm{L\,min^{-1}}$)	4
ZEP3	2 Mar 15:20	3 Mar 8:30	Main inlet ($10\,\mathrm{L\,min^{-1}}$) and 5 m PTFE ($9\,\mathrm{L\,min^{-1}}$)	26

The flowrate through the plastic tubing was equal to the flowrate through the analyzer (around $0.03\,\mathrm{L\,min^{-1}}$), as well as an identical analyzer on the same line, that is installed semi-permanently at the station. From 1 March 15:25UTC until 2 March 14:30UTC (ZEP2 period), we utilized a 2 m section of ¼-inch stainless steel tubing, that was heated to 60 °C, and that extended outside through a cable passthrough to a downward-facing inlet above the rooftop protected by a plastic cover. An additional section of 2 m ¼-inch PTFE tubing (unheated) connected the analyzer to the stainless steel section. Finally, from 2 March 15:20UTC until 3 March 8:30UTC (ZEP3 period), the analyzer was connected directly to Zeppelin's main inlet with a 5 m section of ¼-inch PTFE tubing, flushed at approximately $9\,\mathrm{L\,min^{-1}}$. The analyzer also utilized a higher flowrate during the ZEP3 period, similar to the flowrate used at Snow and Fjord ($0.15\,\mathrm{L\,min^{-1}}$). Regular calibrations with the SDM module and Vapourizer were performed during ZEP1 and ZEP2 (Sec. 4.1.1).

Ambient meteorology during the deployment was measured by Zeppelin's permanent automatic weather station, located at approximately 15 m above the main station building. The weather station provides air temperature and humidity (HMP-155, Vaisala), air pressure (PTB210, Vaisala), and wind speed and direction (WMT700, Vaisala) at a 1 min frequency.

During our routine operations at the observatory, we collected daily samples of the snowpack close to Zeppelin, with the exception of 29 February (Table 2). This sampling was done with a methodology similar to the snowpack collection described in Sec. 3.2.

3.5 Discrete sampling of precipitation

We collected precipitation samples at the main campaign location in Ny-Ålesund and at the various distributed sites of the precipitation sampling network (Figure 1a and Figure 4).

In Ny-Ålesund, precipitation sampling was carried out at the top of the west side staircase of the Marine Laboratory building (78.92731°N, 11.93064°E) at about 5 m above ground and sea level (Figure 1c, "P"). The sampling site is sheltered to the east by the upper two stories of the Marine Laboratory. These measurements complement the continuous weekly precipitation sampling at Ny-Ålesund conducted by the Norwegian Polar Institute (Divine et al., 2011).

In Longyearbyen (LY), precipitation was collected on the roof of the University Centre in Svalbard campus building (78.22262° N, 15.65251° E), approximately 12 m above the local terrain (23 m a.s.l.). Once a day, given a sufficient amount of fresh snow, that snow was collected and homogenized, with an aliquot taken for analysis.

In Tromsø (TR), precipitation sampling took place at three different locations. Firstly, the daily sampling location was on the roof of the Meteorological institute, Vervarslinga for Nord-Norge (69.65384°N, 18.93672°E), at approximately 20 m above the ground (120 m a.s.l.). Secondly, higher-frequency sampling (up to every 3 hours) was done during weekdays at the roof of Teknologibygget of the University of Tromsø (69.68148°N, 18.97846°E) at 30 m above ground (60 m a.s.l.). Thirdly, high frequency sampling during weekends and high frequency sampling on all days after 12 March 2020 took place in a garden in Ramfjordbotn (69.52292°N, 19.24701°E) at ground level (23 m a.s.l.).

In Andenes (AN), sample collection was done in cooperation with the Cold-Air Outbreaks in the Marine Boundary Layer Experiment (COMBLE) field campaign (Geerts et al., 2021). The campaign conducted a combination of daily and high-frequency sampling beside Nordmela harbour (69.137°N, 15.672°E) at approximately 10 m a.s.l.. The sampling location is described in detail in Sodemann et al. (2020).

Near Ålesund (AL), at Barstadvik (62.36019°N, 6.26959°E) the sample collector was installed at ground level (9 m a.s.l.) in an open area with low vegetation. Precipitation was collected on a daily basis, with additional higher-frequency sampling periods.

In Bergen (BG), precipitation samples were collected on the roof of the Geophysical Institute (60.38368°N, 5.33191°E) at the University of Bergen approximately 30 m above the ground (46 m a.s.l.) until 12 March 2020. After 12 March, sample collection was moved about 2.5 km away to the Årstad borough of the city (60.36433°N, 5.35079°E), at ground level (46 m a.s.l.).

Since protocols were kept consistent across the different sites, the sampling procedures described here apply to all sites. Precipitation samples for daily and high-frequency sampling were collected in a clear polypropylene box (approximately 60x40x40 cm LxWxH). Plastic boxes were inspected for precipitation accumulation at regular intervals, at least daily. When heavier precipitation was forecasted for particular sites, sampling frequency was increased if possible. Higher-frequency sampling periods were termed intensive observational periods (IOPs). In total, 2 IOPs were conducted, yielding higher-frequency sampling at Ny-Ålesund, Tromsø, Andenes, and Ålesund (Figure 4). Upon collection end of daily or IOP sampling, the active collection container was swapped with an identical clean and dry replacement container to minimise gaps in the sampling

period and prevent carry-over of sample material. In the case of solid precipitation, sample material was transferred to a plastic sample bag (58 mL Whirl-Pak, Nasco Sampling) with a clean and dry plastic spoon. If the volume of snow exceeded bag size, the box contents were homogenized and an aliquot (i.e. small representative sample) was collected. After melting, the liquid water was poured into an 8.0 mL glass vial (548-0821, VWR International, LLC.) and immediately capped with rubber seal caps. In case of liquid or mixed-phase precipitation, the same plastic container and sampling protocol was used for collection, except that the liquid water would be directly transferred to an 8.0 mL glass vial. For the majority of samples, collecting personnel at all sites noted the weather conditions at time of collection, alongside temperature and wind speed, if available. A summary of precipitation samples collected in Ny-Ålesund during the field experiment is given in Table 2, with overviews of other collection locations found in Figure 4.

4 Data processing, uncertainties and dataset description

4.1 ISE-CUBE data processing

As described in Seidl et al. (2023), the ISE-CUBEs produce two independently logged data streams, one from the CRDS analyzer containing the water isotope data, and another from the profiling arm.

4.1.1 CRDS analyzer data processing

Correction and calibration of the raw measurement signal from the ISE-CUBE system is required to obtain reliable data referencing to the VSMOW-SLAP scale (IAEA, 2009). Calibrations for the Snow and Fjord deployments were performed immediately before and after each deployment of the profiling system at the Marine Laboratory in Ny-Ålesund. The secondary standards DI ($\delta^{18}\mathrm{O} = -7.68 \pm 0.07\,‰$) and ($\delta\mathrm{D} = -49.7 \pm 0.4\,‰$) and GSM1 ($\delta^{18}\mathrm{O} = -32.90 \pm 0.05\,‰$) and ($\delta\mathrm{D} = -261.6 \pm 0.3\,‰$), in use at FARLAB at the University of Bergen, Bergen, Norway, were utilized for calibration. GSM1 represents the most depleted working standard available at the time at FARLAB, but was subsequently replaced by the GLW working standard for liquid water analysis (see Sec. 4.4) and for characterizing the instrument's isotope ratio and mixing ratio dependency (see below). Similarly, DI2 replaced DI, with both being of comparable isotopic compositions. During the experiment, the DI and GSM1 standards were provided to the analyzer with a Picarro Standard Delivery Module (SDM) (A0101, Picarro Inc., USA) and the Vaporizer module (A0211, Picarro Inc., USA), while a Drierite cartridge (MT400, Agilent Technologies Inc., USA) provided dry air. A detailed account of the calibrations preceding and following the Snow and Fjord deployments can be found in Seidl et al. (2023).

During the deployment at Zeppelin, the SDM/Vaporizer combination was used again with the same standards. Thereby, calibrations were conducted every 9 hours between 29 February and 2 March. Each calibration cycle lasted around 1 hour, and consisted of two segments of 20–25 min duration for each standard. A segment was considered valid for calibration if the exposure contained at least 10 consecutive minutes with humidity variation below 0.3 g/kg (500 ppmv). As was also the case for the calibrations performed at the Marine Laboratory, the standard deviation of the mean isotopic values across the 5

calibrations was smaller than the isotopic standard deviation experienced during any individual exposure, for both δ^{18}O and δD. Furthermore, the calibrations at Zeppelin and for the entire campaign exhibited negligible drift (less than 0.01 (δ^{18}O) and 0.02 (δD) ‰ per day, see Seidl et al. (2023)).

Calibration of the water vapour isotope measurements were also obtained using the long-term slope and offset of the analyzer's raw δ^{18}O and δD signals compared to secondary standards calibrated at FARLAB onto the VSMOW-SLAP scale. Previous deployments have shown that the type of CRDS analyzers used here have a long-term drift that is similar to the measurement precision (Bailey et al., 2023). We observe this also to be the case for the specific analyzer used here (Ser. No. HIDS2254) over a time frame of several years. In the selection of valid calibration runs, calibration segments of typically 20 min from an SDM were retained if the mixing ratio was between 18'000 and 30'000 ppmv, while low-quality calibration runs with oscillations of the water concentration due to bursting air bubbles were excluded. Calculated from more than 1000 calibrations with different secondary laboratory standards performed in the period from 20 Nov 2016 to 30 May 2022 in laboratory application and field deployments, we find mean slope and offset values of:

$$\delta^{18}\mathrm{O}_{cal} = 1.1169 \times \delta^{18}\mathrm{O}_{raw} + 0.7742 \quad ‰$$

$$\delta\mathrm{D}_{cal} = 0.9163 \times \delta\mathrm{D}_{raw} - 8.3058 \quad ‰$$

These calibration coefficients have been obtained from a linear regression to the long-term average values of 6 secondary standards calibrated to the VSMOW-SLAP scale. From the standard deviation about the regression, the calibration uncertainty for a sample at -10 ‰ (δ^{18}O) and -100 ‰ (δD) is thereby estimated as 0.44 ‰ and 1.5 ‰, respectively. These long-term calibration values only shifted markedly when the analyzer was returned from service at the manufacturer after June 2022. Calibrated water vapour isotope data from this approach are denoted by appending the suffix "_LT" to the respective data variables (see Table A1).

During the ISLAS2020 field deployment, consistency with the long-term calibration coefficients was checked from SDM calibrations performed in a laboratory environment. The median absolute difference between the two calibration methods for the entire experiment is 0.10 ‰ for the δ^{18}O and approximately 1.0 ‰ for δD. Uncertainty has possibly been introduced in these field calibrations due to remnant humidity in the background air that was dried with a moisture trap.

For both calibration methods, the accuracy of CRDS isotopic measurements is subject to a dependency on both isotope ratio and mixing ratio (Aemisegger et al., 2012; Bonne et al., 2014; Weng et al., 2020). Since the response is often particularly pronounced at low mixing ratios, it is crucially important for the ISLAS2020 field deployments to perform correction for this dependency. Response characteristics are different for each specific analyzer, and can be determined from providing a vapor stream of a known isotopic composition across a wide mixing ratio span. For the particular CRDS analyzer used in ISLAS2020, such a characterization was performed first in 2018 using autosampler injections of laboratory standards (Weng et al., 2020). The characterization has since been repeated several times and updated with a wider range of standards, including a standard more depleted (GLW) than the one used for calibrations during the campaign (GSM1) (see Sec. 4.4). Here we use the correction method based on a large number of suitable characterisation measurements, involving a calibration device based on microdrop dispensing technology (Sodemann et al., 2023a). The correction for the ISLAS2020 campaign (Figure A1) is largest for low

mixing ratios that are more depleted (less than -247.9 ‰ δD and -27.95 ‰ δ18O for mixing ratios below 0.6 $\mathrm{g\,kg^{-1}}$). 38.6 % of the measurement dataset fall in this range. The median correction for this subset is -10.1 ‰ for δD and 1.01 ‰ for δ18O, while the median correction for the entire dataset is -6.5 ‰ for δD and 0.60 ‰ for δ18O. In particular at the lowest depletion and mixing ratios, the correction has a significant impact on the d-excess, and introduces uncertainty. Estimates from a bootstrap method give an uncertainty of 0.4 ‰ for δD and 0.1 ‰ for δ18O for this correction (Sodemann et al., 2023a).

Variables relating to CRDS measurements can be found in Table A1 for each deployment under the "CRDS analyzer" grouping. CRDS analyzer variables are available at a 30 s resolution in the data files from Snow and Fjord (see Seidl et al. (2023)), whereas Zeppelin resolution is 2 min.

4.1.2 Profiling arm data processing

The profiling arm monitored and logged the ambient temperature just beside the sampling inlet, as well as the height of the inlet above the underlying surface. A temperature offset of $+0.67\,^{\circ}\mathrm{C}$ was identified from laboratory testing and accounted for in the final data set. Distance sensors onboard the profiling arm were also routinely compared with manual measurements and found to be accurate to within 2 cm. Full details of the data processing can be found in Seidl et al. (2023). Variables relating to the profiling arm measurements can be found in Table A1 for the Snow and Fjord deployments under the "Profiling module" grouping. Similarly to the CRDS analyzer variables, profiling module variables are available at 30 s resolution.

4.2 Ambient meteorological measurement processing

The automatic weather station near the Snow site measured horizontal wind speed and direction, air temperature, and surface temperature. The minimum speed for the propeller anemometers of the AWS is 1.0 $\mathrm{m\,s^{-1}}$ and 1.1 $\mathrm{m\,s^{-1}}$ for determining wind direction, resulting in increased uncertainty of winds below these thresholds. The surface temperature (T_s) is calculated from the Stefan-Boltzmann law from radiative flux measurements using a surface emissivity $\epsilon = 0.985$ which is typical for snow. Changing ϵ by 0.005 results in variations of approximately 0.3 K The data from the AWS is associated with the variables listed under the "Meteorological station (S)now" of Table A1, and are available at 30 s resolution.

The eddy-covariance station installed at the Fjord site was primarily utilized to provide both the horizontal wind and air temperature at the measurement site. Wind and temperature data was quality controlled according to the internal diagnostic flagging of the sonic anemometer. Converting measured wind speeds from the instrument's local coordinate system into geographic coordinates included correcting external offset from true north (21° NNE). Atmospheric pressure measurements from the open path gas sensor required no additional processing. Once quality controlled and direction corrected, the 20 Hz signal from the station was aggregated to 30 s averages to match with the CRDS and profiling module measurements. Wind, temperature, and pressure measurements from the eddy-covariance station are connected to the variables in the "Meteorological station (F)jord" category of Table A1.

The Zeppelin weather station provided air temperature, relative humidity, atmospheric pressure, and horizontal wind speed and direction with associated quality scores for each. For the entire deployment period, all but the wind variables constantly produced data of maximum quality (score 100). Wind measurements had a few brief episodes of lower quality, but still ranked

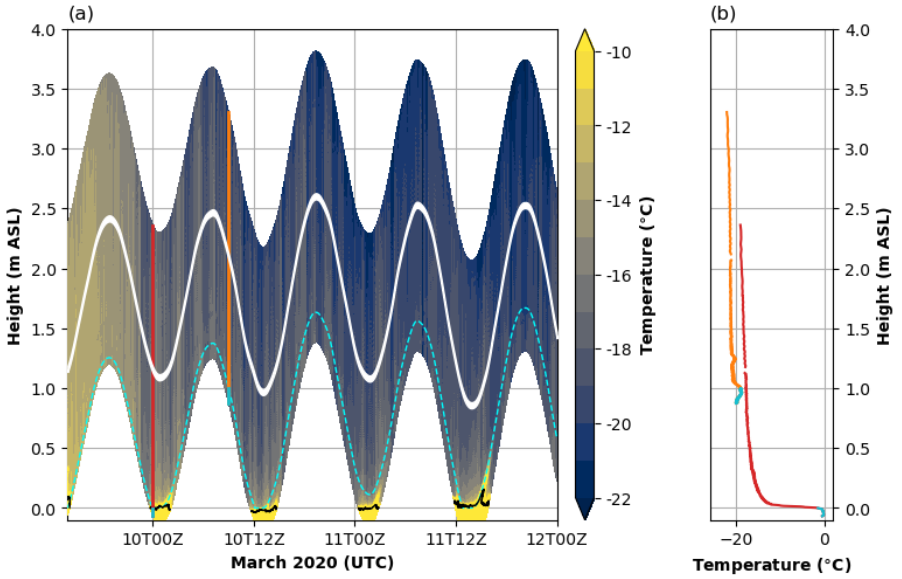

Figure 6. Total timeseries of the temperature observed by the Fjord FODS column (a, shading). White gap in middle of column (a,b) caused by plastic support ring. Black contour (a) is the -1.8 °C threshold, representing the water surface. Dotted cyan line (a) denotes level at which the column has been previously fully immersed in fjord water, and therefore might be prone to icing effects; this does not include the potential icing level caused by wave action, which might extend the effects further up. Red/cyan line (a,b) indicates 10 March 2020 00:00UTC profile, with cyan section showing extent that the column has been previously fully immersed. Orange/gray line (a,b) is the same for 10 March 2020 19:40UTC.

a mean quality of 99.9 for the deployment period. These quality scores, in addition to the parameters themselves, are registered to the variables listed under "Meteorological station (Z)eppelin" in Table A1. Zeppelin weather station data is available at 2 min resolution.

Decomposition of wind speed and direction into northward and eastward components, as well as the conversion from relative to specific humidity was done via the open-source Python software package, MetPy (May et al., 2022).

4.3 Fiber-optic distributed sensing column processing

The FODS instrument for the Snow column recorded temporal averages of 3 s. Since the instrument consecutively sampled three different fibers, samples have an effective temporal resolution of 9 s. For the Fjord FODS the instrument recorded temporal averages over 10 s; further details on accuracy and bias for both columns can be found in Zeller et al. (2021) and Thomas et al. (2022). Signal handling and datalogging at the Snow site utilized an ULTIMA DTS, 5 km variant (Silixa, UK), whereas the Fjord deployment had an XT DTS (Silixa, UK). These instruments resolve temperature measurements along the fiber-optic cable about every 0.6 m. As the circumference of the glass-mesh support is approximately 1 m, transforming this signal into a vertical profile involves converting the length along the fiber into a number of wraps around the glass-mesh according to the

spacings given in Sec. 3.2. Each height level was then averaged over 30 s intervals, producing a dataset with the same time resolution as the ISE-CUBE data.

The surface properties of the two sites required different treatment at the lowest heights of the column data. At the Snow site, the column was partly in the snowpack. The average snow height above the bottom of the column was 0.17 m during that time period, which is subsequently used as the "zero-level" in the dataset. Averaging over a band ±0.005 m on either side of the zero-level gives the temperature in the surface snow (in the dataset as "Tsnow"), a bulk measure of the temperature across the snow-air interface.

At the Fjord site, due to the tidal variations, determining a zero-level for the water's surface was more involved. At times during the deployment, the bottom-most 0.25 m was immersed in the fjord water. The timing of this immersion matches with the semi-diurnal high tide mark. We utilized the observed tidal height for Ny-Ålesund from Kartverket[1], interpolated to a 30 s resolution. Using a -1.8 °C temperature threshold (Figure 6a, black contour) as a guide for surface level, we qualitatively matched the immersed signal with the tidal signal. This allowed to calculate the time-dependent distance between the surface of the water and the bottom of the column, and the resulting temperature gradient (Figure 6a, shading). Owing to the immersion capability of the FODS column, we can clearly distinguish the surface of the water at 00UTC on 10 March (Figure 6, red/cyan line). However, the immersion also led to ice buildup at air temperatures below freezing, which is evident in the temperature anomaly in the lower levels at 09UTC (Figure 6, orange/cyan line).

Data from the FODS columns from the Snow and Fjord deployments are listed with the variables found in Table A1 under the "FODS column" grouping.

4.4 Laboratory analysis of liquid samples

In total, 202 samples of freshwater (rain, snow and surface snow) and seawater were collected during the ISLAS2020 campaign, across all campaign locations. All collected samples were analysed within weeks after collection at the Facility for Advanced Isotopic Research and Monitoring of Weather, Climate and Biogeochemical Cycling (FARLAB) at the University of Bergen. The analysis was done by liquid injections on two Picarro L-2140i CRDS analyzers (Picarro Inc, Sunnyvale, USA; Ser#: HKDS2038 and HKDS2039), utilizing Picarro Autosamplers (A0340) and Vaporizers (A0211). Secondary laboratory standards (Table 6) were thereby used to account for instrument drift, as well as for calibration of samples onto the VSMOW-SLAP reference scale using the analytical sequence described in the Appendix of Sodemann et al. (2023b). The secondary standards GLW and EVAP2 were utilized for freshwater sample calibration, with DI2 and FIN serving as drift standards. EVAP2 and DI2 were used for saltwater calibration with BERM used as a drift standard (Table 6). The software package FLIIMP (FARLAB liquid injection isotope measurements processor) V2.0 was used for corrections and calibration of all samples. Combined uncertainty for each sample is included in the dataset, and comprises the calibration uncertainty of the secondary standards, the repeatability for each sample, and the long-term reproducibility of the measurement system.

[1] https://www.kartverket.no/en/at-sea/se-havniva/result?id=1082348, last accessed: 22 December 2022

Table 6. Secondary lab standards used for the calibration of liquid samples onto the VSMOW-SLAP scale.

Standard name	δ^{18}O (‰)	δD (‰)
GLW	-40.02±0.07	-307.79±0.75
FIN	-11.60±0.10	-80.78±0.47
DI2	-7.63±0.10	-50.72±0.27
BERM	0.62±0.12	6.80±0.51
EVAP2	1.81±0.13	9.52±0.65

5 Data examples

We now present examples of profiling operations from the field experiment, as well as the time-series of precipitation samples from across the collection network. The Python based code used to generate all figures in this Section can be found in the Supplementary material; this code requires the open-source Python software package, MetPy (May et al., 2022). We begin with two examples of profiles from the Snow and Fjord sites.

5.1 Profiling sites

The example from the Snow site spans 4.5 h on 28 Feb 2020 (Figure 7). The temporal variation of the inlet height (Figure 7a, black line with red highlight) is set against the backdrop of the vertical temperature profile from the FODS column (shading). The snow temperature (blue line) and surface temperature (cyan line) were always several degrees below the $2.1\,\mathrm{m}$ ambient temperature (orange line), reflecting the very stable stratification typical of the Snow site (Figure 7b). The temperatures at the inlet height extracted from the FODS column (red line) and measured at the sensor head (black line) clearly co-vary (r=0.942), but with a positive bias for the inlet temperature sensor of $1.5\,^{\circ}\mathrm{C}$. The example profile shown was made under light wind conditions with wind speeds under 3 m/s (Figure 7c, orange line). Winds were predominantly from the south (black dots), indicating air descending from the direction of the nearby inland glaciers (Figure 1c). These meteorological observations together set the context for the water isotope measurements (Figure 7d). The surface of the snow during this time period had a water isotopic composition of -135.70‰ for δD, with a d-excess of 27.90‰. The overlying vapour for the same time period was characterized by highly depleted conditions in δD reaching below -370‰ (black line). The d-excess closely followed the time evolution of the δD, albeit at and around very negative values of -40‰. The co-variation between δD and d-excess indicates that the δ^{18}O has a different variability, which is substantially smaller than δD over the different heights of the profile (not shown).

These low d-excess values may initially appear surprising and thus questionable in terms of data quality, however mass balance dictates that kinetic fractionation creates both positive and negative d-excess values as HDO molecules are removed preferentially from a reservoir, such as during condensation flux from the atmosphere to a cold surface. Negative or low d-excess values have, for example, been reported in water vapour measurements in the deep Arctic (Brunello et al., 2024), in the Iceland-Greenland Sea (Sodemann et al., 2024), and over the southern Ocean (Thurnherr and Aemisegger, 2022). Other

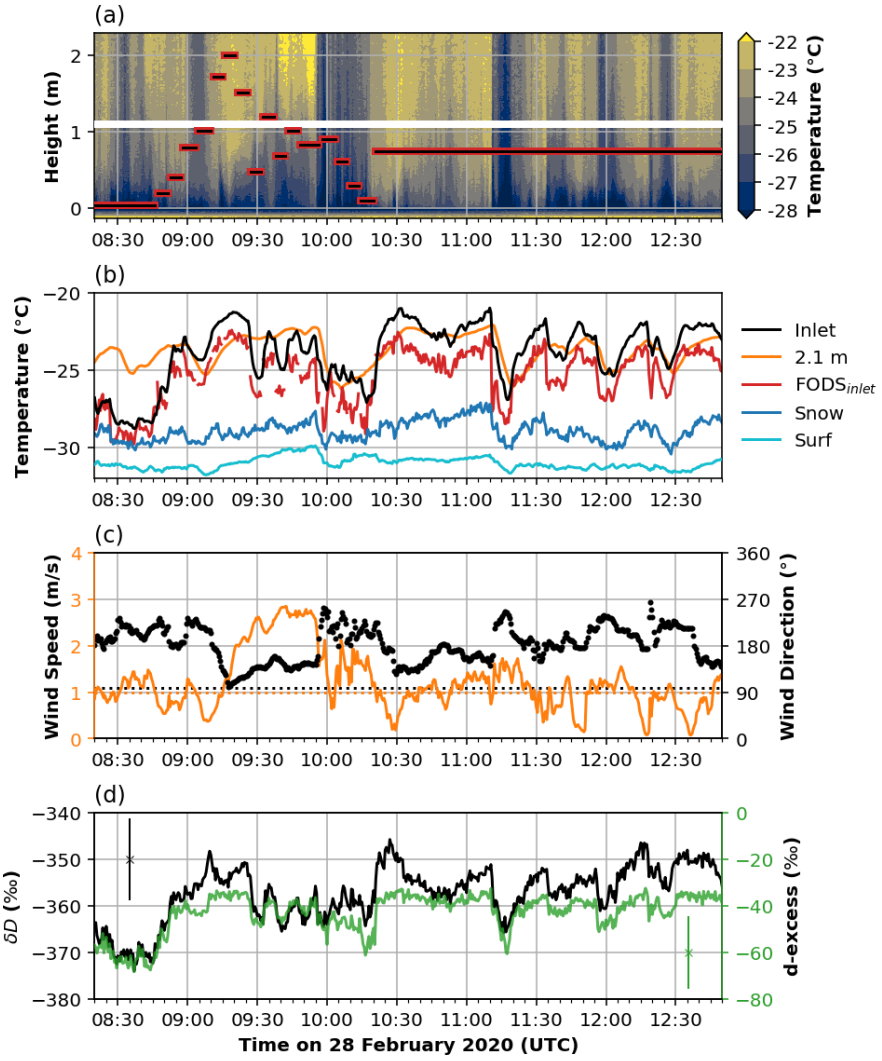

Figure 7. A profiling period from 28 Feb 2020 8:20 to 12:50UTC over snow-covered tundra. (a) Height of sampling inlet (black/red line) displayed alongside temperatures observed with FODS column (shading). White gap caused by plastic support ring. (b) Inlet temperature (black), 2.1 m temperature (orange), and temperature of FODS column at inlet height (red), as well as snow (blue) and surface (cyan) temperature. (c) Wind speed (left axis, orange) and wind direction (right axis, black). Dotted lines indicate manufacturer's detection thresholds (i.e. minimum wind speed) for wind speed (dotted red) and direction (dotted black). (d) δD (left axis, black) and the d-excess (right axis, green). Representative scale for the variability in isotopic measurement at any one data point given for δD (left, black) and d-excess (right, green).

studies have interpreted negative d-excess values as potentially being caused by sublimation effects (Hu et al., 2022). Wind-tunnel experiments with blowing snow have indicated that deposition onto blowing snow could lower the d-excess of the water vapour (Wahl et al., 2024). The d-excess measurements shown here have been made in an environment close to open water, where it is plausible that air masses advected over nearby cold surfaces can induce deposition fluxes to the surface that lower the d-excess in atmospheric water vapour. A forthcoming study will investigate this hypothesis in more detail.

The example from the Fjord case covers 5.5 h during 10 Mar 2020 (Figure 8). In contrast to the Snow site, the temperature gradients observed by the FODS column over water are characterized by warm air close to the water surface, overlaid by colder air (Figure 8a). There are clear co-variations between air temperature measurements from the inlet (black line), from the FODS column at inlet height (red line), and from the sonic anemometer (orange line) (Figure 8b). At the Fjord site, ambient temperatures were almost always (97.9 % of the deployment) colder than the inlet temperature, with most of the remaining time occurring during higher windspeeds (> $5\,\mathrm{m\,s^{-1}}$) than those typically encountered during profiling. For the profiling period shown, wind speeds were relatively low (about $2\,\mathrm{m\,s^{-1}}$) and with mainly southerly directions (Figure 8c). The corresponding measurements in isotope parameters show pronounced variation with height (Figure 8d). Above the surface of the water (δD=0.3 ‰, d-excess=0.9 ‰), at 3.5 m or higher, the δD reached below -280 ‰ (before 9:10UTC and around 10:45UTC), while at lower levels the δD was substantially less depleted (about -200 ‰). The d-excess (black line) follows again closely along the pattern of the δD, yet at this location it exhibits predominantly positive values, except for the periods where the inlet was above 3.5 m height. We interpret this strong vertical gradient in the lowermost metres of the boundary layer as a signature of two very different airmasses meeting at the Fjord site, where the upper layer begins to resemble the conditions at the Snow site, and the lower layer is influenced by surface evaporation. Further analysis of these differences can provide insight into the isotopic fractionation occurring between atmosphere and surface, namely during evaporation from, and deposition onto, the surface.

5.2 Precipitation collection

Figure 9 shows the time series of the isotopic composition of precipitation collected during the campaign, from across the sampling network. The distance of the sampling location from Ny-Ålesund increases from the top to bottom panel. Grey shading indicates the two IOP periods of the campaign. There are variations in both the δD (black lines) and d-excess (green lines) that vary with the prevailing weather conditions, namely the WAI and different CAOs (Figure 2). More northerly locations tend to have more variable water isotope composition, with Ny-Ålesund (Figure 9a) exhibiting the largest standard deviation (δD_{stdev}=64.0 ‰, d-excess$_{stdev}$= 13.0 ‰), and Bergen (Figure 9f) the lowest (δD_{stdev}=24.8 ‰, d-excess$_{stdev}$= 3.8 ‰). Trends also appear in the mean isotopic depletion, which becomes more negative in the poleward direction, and the d-excess values, which become more positive. A statistical overview of the precipitation isotope composition from the sampling network can be found in Table 7.

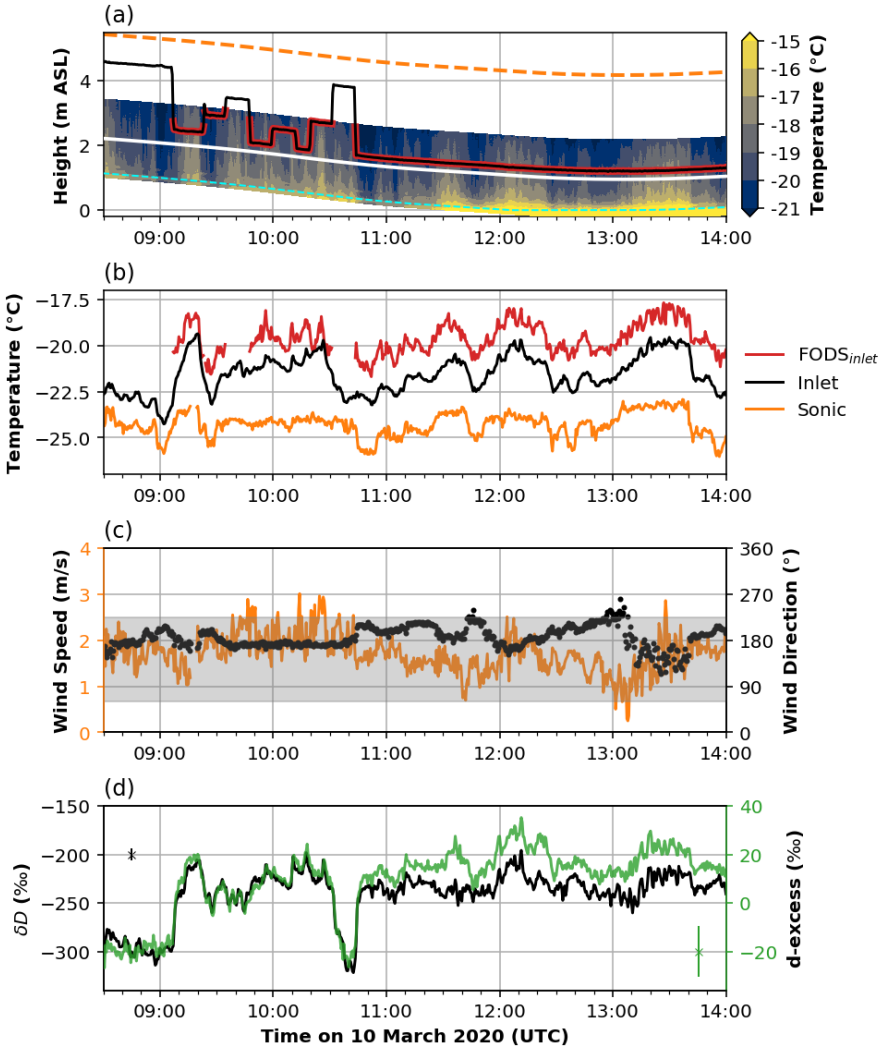

Figure 8. A profiling period from 10 Mar 2020 8:30 to 14:00UTC over open fjord water. (a) Height of sampling inlet (black/red line) displayed alongside temperatures observed with FODS column (shading). White gap caused by plastic support ring. Dashed cyan line indicates previous/current immersion level, similar to Figure 6a. Dashed orange line is the height of the sonic anemometer, above sea level. (b) Inlet temperature (black), sonic temperature (orange), and temperature of FODS column at inlet height (red). (c) Wind speed (left axis, orange) and wind direction (right axis, black). Grey shading indicates the sector where the inlet is in the wind shadow of the concrete pier that it is deployed upon. (d) δD (left axis, black) and the d-excess (right axis, green). Representative scale for the variability in isotopic measurement at any one data point given for δD (left, black) and d-excess (right, green).

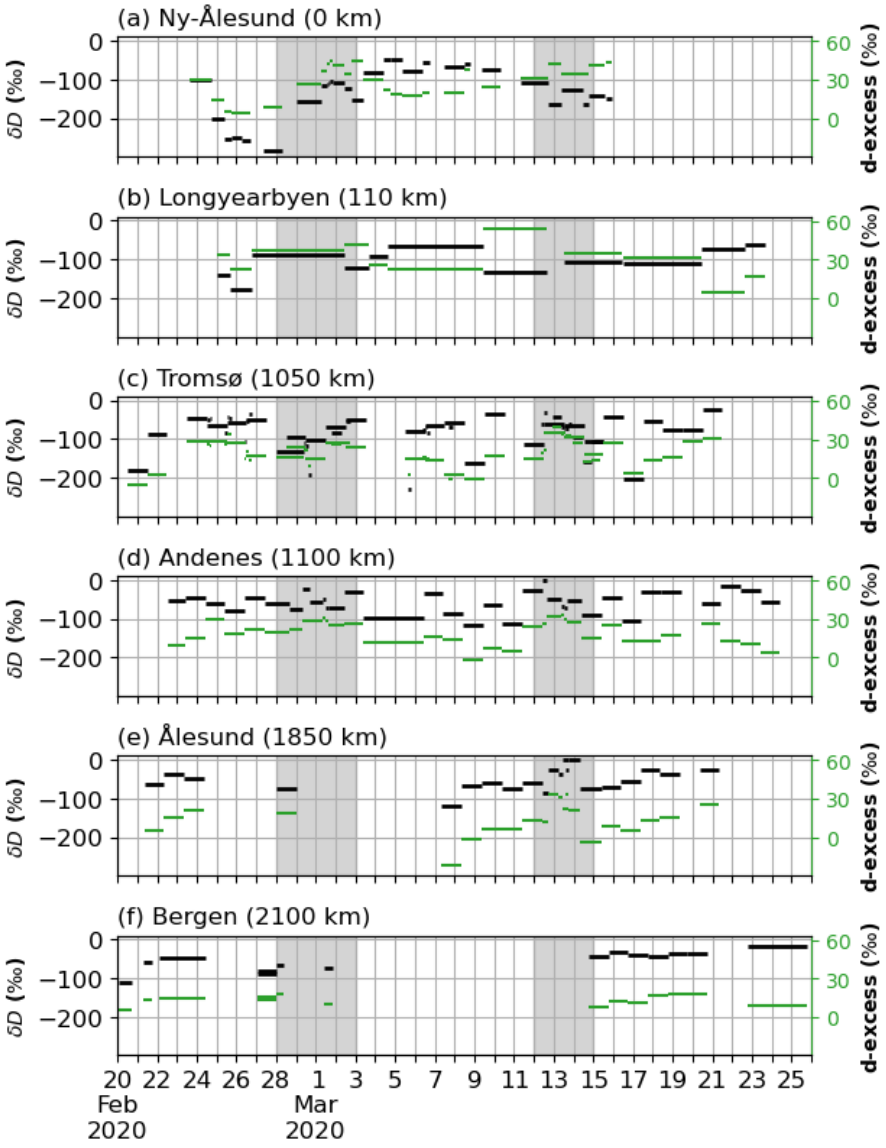

Figure 9. Isotopic values of precipitation collected during the campaign. Left axis (black) indicates δD, whereas right axis (green) indicates the deuterium excess. Locations are as follows, with approximate distance from Ny-Ålesund given in brackets: (a) Ny-Ålesund, (b) Longyearbyen, (c) Tromsø, (d) Andenes, (e) Ålesund, and (f) Bergen. Grey shading indicates the two IOP periods for precipitation sampling.

Table 7. Statistics for isotopic composition of collected precipitation across the sampling network locations. The notation for the d-excess has been shortened to "d" in the table below.

Sampling location	Distance to Ny-Ålesund (km)	$\delta D_{mean} \pm \delta D_{stdev}$ [δD_{min} , δD_{max}] (‰)	$d_{mean} \pm d_{stdev}$ [d_{min}, d_{max}] (‰)
Ny-Ålesund	0	-130.6 ± 64.0 [-282.5, -46.8]	29.1 ± 13.0 [4.1, 45.0]
Longyearbyen	110	-107.1 ± 33.8 [-177.8, -61.3]	29.4 ± 12.5 [4.4, 53.5]
Tromsø	1050	-83.3 ± 44.5 [-229.7, -22.7]	20.1 ± 10.4 [-4.9, 39.2]
Andenes	1100	-58.0 ± 27.6 [-118.2, -0.1]	19.5 ± 9.0 [-1.3, 33.0]
Ålesund	1850	-50.6 ± 28.1 [-117.8, 0.4]	13.3 ± 12.9 [-21.9, 33.67]
Bergen	2100	-55.7 ± 24.8 [-111.0, -16.8]	12.9 ± 3.8 [5.0, 17.6]

6 Discussion

In this section, we first present some of the limitations and potential sources of uncertainties in our campaign dataset before discussing possible synergy between both our local and regional observations, and additional instrumentation from additional scientific investigators.

6.1 Measurement uncertainties and limitations

As with other measurements in a challenging field environment, our dataset has sources of uncertainty that can impose limitations for use and interpretation. Foremost, the low humidities encountered during the experiment impart an elevated level of uncertainty to the water vapour isotope measurements. Higher uncertainty stems from the twofold effect of the decreased precision of the analyzer at low humidities and the mixing ratio-isotope dependency attributed to the instrument, which is especially pronounced at low humidities (Aemisegger et al., 2012). The mixing ratio-isotope ratio dependency can be accounted for by a thorough characterization device before and after deployments (Sec. 4.1.1) (Sodemann et al., 2023a) while the lower precision is inherent to the analyzer and can only be mitigated by measurement strategy, such as averaging times. As described in Seidl et al. (2023), each height interval of the profile lasted for a minimum of 4 minutes. Together with the increased flow rate through the measurement cavity of the analyzer, this strategy results in a more robust statistical average for each height level, and therefore a more resolved profile. However, the FODS column data shows wind events that rapidly change the vertical temperature structure at both sites, indicating transient eddies persiting for many times shorter than the duration of our profile

itself. This both highlights the inability of our system to resolve the individual eddies, and points to the potential for the FODS column to provide additional constraints when analysing the water isotopic data.

In addition, flow distortion around the profiling sites might have impacted surface exchange processes during the experiments. To address this possibility, the profiling equipment used was designed with a minimal volume (Seidl et al., 2023), and the profiling arm was orientated such that it was directed upstream of the equipment. This approach did appear to work as intended during the Snow deployment, where prevailing southerly winds met the south-westerly pointing arm unimpeded. At the Fjord site, however, flow distortion proved to be unavoidable. The large concrete pier (orientated NE-SW) sheltered the profiling inlet during south-easterly winds (Figure 8, grey shading), and served as an impassable "back-stop" to the profiling inlet during north-westerly winds, introducing flow convergence and turbulence to the sampling site. As profiling was limited to lower wind speeds, the impact of this flow distortion at the Fjord site is deemed to be limited, but not negligible.

Additional profile measurements at both sites or similar locations would therefore be highly desirable, and more easy to attain given the experience documented here and elsewhere (Seidl et al., 2023).

Winds and flow distortion are also a potential source of uncertainty for the precipitation samples collected for water isotope analysis. Snow drift and undercatch of snow are well-known problems for precipitation collection in general (Wolff et al., 2015). For water isotope analysis, the undercatch is a less severe problem than the introduction of previously fallen, loose surface snow into the collector. Additionally, the prompt collection of precipitation before collection is another important factor when it comes to limiting post-depositional modification of the isotopic signal (e.g. Hughes et al., 2021; Aemisegger et al., 2022; Casado et al., 2021; Wahl et al., 2024). During the campaign, a consistent sampling protocol and the available additional metadata on wind conditions allows for identification of samples that could be affected by such post-depositional effects.

6.2 Opportunities for coordinated analysis

Owing to the nature of the Ny-Ålesund experiment site, there are additional complementary datasets from instrumentation present in and around the settlement, a select few of which we present here. Firstly, there is the entirety of the horizontal FODS array from the NYTEFOX experiment, including multiple sonic anemometers (Zeller et al., 2021; Huss et al., 2021). As this horizontal array also gives information on wind speed and direction, there is potential to analyze how fine-scale advection could impact water vapour isotope composition. Such effects can in particular be visible while the profiling arm was stationary for longer periods of time, such as during overnight periods. Such measurement periods highlight the dynamic advantage of our articulating profiling system over switching manifold installations (Steen-Larsen et al., 2013; Berkelhammer et al., 2016; Wahl et al., 2021) as we were able to readily focus our measurements at particular heights of interest, on-the-fly. In addition, insights into the larger vertical structure of the atmosphere is provided by radiosonde launches 4 times daily, alongside remote sensing of temperature, humidity, and winds. Furthermore, an identical CRDS analyzer was installed at Zeppelin throughout the ISLAS2020 campaign, with both instruments sampling from the same inlet during the first stage of our deployment at Zeppelin (ZEP1). Interested data users are encouraged to contact any of the Principal Investigators for this data collection for more details on these additional data sources.

The ISLAS2020 field experiment took place while the large, international MOSAiC drift campaign took place in the Arctic (Shupe et al., 2022). Since the MOSAiC drift, lasting from October 2019 to September 2020, also involved water isotope measurements in vapour, precipitation, sea ice and other components (Brunello et al., 2023), there is a potential to find situations where warm airmasses that intruded into the Arctic (Figure 2b) over Ny-Ålesund were later encountered by MOSAiC instrumentation (Brunello et al., 2024). Vice versa, cold and dry airmasses that left the Arctic during the different CAO periods may have been over the MOSAiC site beforehand (Figure 2c). The precipitation samples from our collection network may be related to both the ISLAS2020 experimental site measurements and MOSAiC experiment in similar ways. In either case, atmospheric transport modelling using tools such as the FLEXible PARTicle dispersion model (FLEXPART) (Pisso et al., 2019), are needed to determine the likelihood of connection between different sampling sites. With sufficiently high probability of connection, associated samples can then give information about the transformation of airmasses entering and leaving the Arctic.

7 Summary and Conclusions

In this data paper, we describe and summarize the aims, instrumentation, and measurement activities conducted during the ISLAS2020 campaign from 20 Feb to 25 March 2020, with a particular focus on the field experiment at Ny-Ålesund (78.9° N, 11.9° E), Svalbard, Norway from 23 Feb to 15 March. We describe the setting of the campaign and the variable weather conditions encountered during this exceptionally cold spring period. The primary aim of the field campaign/experiment was to acquire near-surface profiles of the vapour isotope composition over different Arctic surface conditions to characterize surface exchange processes of water vapour at these latitudes. To this end, we deployed high-resolution profiling equipment over snow and over the partially ice-covered fjord environment. Our secondary objectives included contextualizing these profiles, both vertically and at a larger horizontal scale. Vertically, the isotopic state of the free troposphere was briefly observed between profiling deployments, while on a regional scale, a wider network of discrete precipitation samples can be used to analyze the field experiment in terms of upstream/downstream measurements. This data paper serves as a reference document for the deployed instrumentation, dataset location, processing and calibration, auxiliary datasets, and data availability. Furthermore, we provide several examples for the intended use of the dataset.

Water vapour isotope measurements at these high latitudes and weather conditions are challenging in several aspects. This includes the low absolute humidity, which increases noise of the CRDS instrumentation, and overall cold conditions, which also requires non-standard approaches to calibration methods. Nonetheless, as demonstrated by the examples, the dataset is of overall entirely sufficient quality and comprehensiveness to allow scientific studies related to exchange processes over snow, sea ice, and open water in extreme, high-latitude environments focused on both process understanding and model development and verification. The additional precipitation and other discrete water samples furthermore allow to place the local water vapour isotope measurements into the context of other measurement activities with respect to the origin and destination of Arctic water vapour and the ensuing transformations as recorded by its water isotope composition, including the MOSAiC campaign.

8 Data availability

Data from the ISLAS2020 campaign can be accessed at the PANGAEA data repository at doi.org/10.1594/PANGAEA.971241 (Seidl et al., 2024). The data collection has been divided into datasets focusing on continuous (netCDF) and discrete (CSV) sampling. Continuous sampling has been subdivided by deployment period. Each of the three deployment periods has a corresponding netCDF file containing the continuous parameters measured during that time. Missing time intervals at Zeppelin coincide with instrument calibration or the switching of inlets. Missing time intervals at Snow or Fjord coincide with instrument error/failure. The complete 20 Hz dataset from the eddy covariance station is also made available for interested data users. An overview of data availability for the continuously sampled variables at the three deployment sites can be found in Figure 3.

Data from discretely collected water samples is found in a tab-delimited file. In addition to the isotopic analysis for each sample, every discrete sample is associated with metadata relating to its collection. This collection metadata includes the time period, location, and type of water sample. Samples taken in Andenes can also be found as a part of the COMBLE campaign dataset (Sodemann et al., 2020). An overview of data availability for the discretely collected water samples variables for the entire campaign can be found in Figure 4.

Some of the instrumentation included in the ISLAS2020 datasets extend beyond the time period covered in the dataset file, namely the ambient meteorological conditions from the Snow and Zeppelin weather stations, and the full installation period of the Snow FODS column. Corresponding time periods of data availability are indicated with light shaded bars in Figure 3. Principal investigators for these expanded data sources can be found in the metadata of the respective dataset file.

Appendix A: Additional information

As described in Sec. 4.1.1, the specific isotope analyzer used in the field has to be characterized for an isotopic measurement response which is dependent on mixing ratio. Figure A1 shows this characterisation surface for Picarro L2130i (Ser#: HIDS2254).

For reference, the variables in the ISLAS2020 dataset are provided in Table A1, arranged by source instrument/instrument group. These variables are cross-indexed with the available deployment site location, denoted by S, F, and Z (Snow, Fjord, and Zeppelin, respectively).

Author contributions. Data collection: All authors; Dataset processing: AWS, AD, HS, JMH, CKT, AS, OH; Writing – original draft preparation: AWS, AJ, JMH, HS; Writing – review and editing: All authors

Competing interests. The authors declare no conflict of interest. The funders had no role in the design of the study; in the collection, analyses, or interpretation of data; in the writing of the manuscript, or in the decision to publish the results.

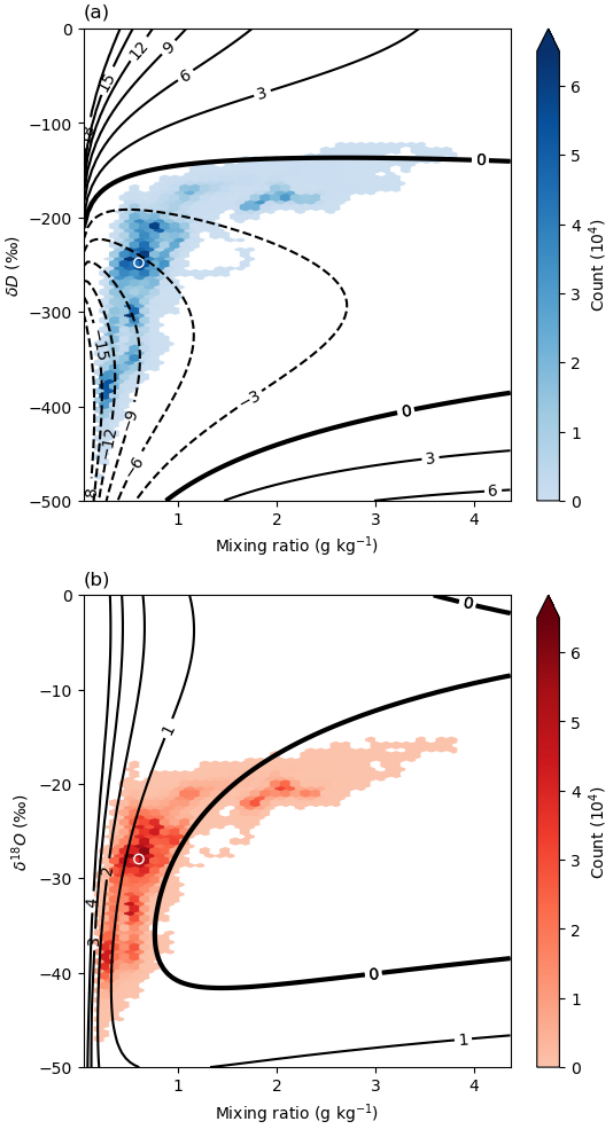

Figure A1. Isotope–mixing ratio correction surfaces for δD (a) and δ^{18}O (b) for the Picarro L2130i (Ser#: HIDS2254) used during the ISLAS2020 field experiment. Contour values denote the correction value needing to be added to raw data. Colored shading denotes concentration of data points from the raw ISLAS2020 dataset. The white circle indicates the median of the dataset for both isotopic value and mixing ratio.

Table A1. Names of variables in datasets from Snow (S), Fjord (F), and Zeppelin (Z) deployment sites.

Grouping	Variable	Dataset(s)	Grouping	Variable	Dataset(s)
CRDS analyzer	delta_18O	S, F, Z	Meteorological station(s)	Ta	S, F, Z
	delta_18O_SD	S, F, Z		Ta_SD	S, F, Z
	delta_18O_LT	S, F, Z		FF	S, F, Z
	delta_18O_LT_SD	S, F, Z		FF_SD	S, F, Z
	delta_D	S, F, Z		UU	S, F, Z
	delta_D_SD	S, F, Z		UU_SD	S, F, Z
	delta_D_LT	S, F, Z		VV	S, F, Z
	delta_D_LT_SD	S, F, Z		VV_SD	S, F, Z
	d	S, F, Z		p_aws	F, Z
	d_SD	S, F, Z		p_aws_SD	F, Z
	d_LT	S, F, Z		Ta_050_cm	S
	d_LT_SD	S, F, Z		Ta_100_cm	S
	q	S, F, Z		Ta_150_cm	S
	q_SD	S, F, Z		FF_050_cm	S
	p	S, F, Z		FF_100_cm	S
	p_SD	S, F, Z		FF_150_cm	S
	Tc	S, F, Z		UU_050_cm	S
	Tc_SD	S, F, Z		UU_100_cm	S
	pc	S, F, Z		UU_150_cm	S
	pc_SD	S, F, Z		VV_050_cm	S
	Twb	S, F, Z		VV_100_cm	S
	Twb_SD	S, F, Z		VV_150_cm	S
	Tdas	S, F, Z		Tsurf	S
	Tdas_SD	S, F, Z		Tsurf_SD	S
	crds_flag	S, F, Z		WW	F
Profiling module / Inlet details	inlet_height	S, F		WW_SD	F
	inlet_height_SD	S, F		wind_diagnostic	F
	profile_number	S, F		q_aws	Z
	Ta_inlet	S, F		q_aws_SD	Z
	Ta_inlet_SD	S, F		Ta_q_aws_quality	Z
	direction	S, F		FF_UU_VV_quality	Z
	subdeployment_number	Z		p_aws_quality	Z
FODS column	Tcol	S, F	Kartverket	z_above_water	F
	Tcol_SD	S, F		z_offset	F
	Tcol_inlet	S, F		max_inlet_height	F
	Tcol_inlet_SD	S, F			
	z	S, F			
	Tsnow	S			
	Tsnow_SD	S			

Acknowledgements. We would like to thank all of the Kings Bay staff present in Ny-Ålesund during the ISLAS2020 experiment, especially Marine Ilg at the Kings Bay Marine Laboratory. We also want to acknowledge the hard work and dedication of the additional members of the NYTEFOX field experiment: Marie-Louise Zeller, Lena Pfister, Daniela Littmann, and Johann Schneider. The ISLAS2020 experiment also would not have been possible without the fine infrastructure and hosting provided by the Norwegian Polar Institute, especially Christina Pedersen. Similarly, the entire staff at the joint French–German AWIPEV research station in Ny-Ålesund (operated by the Alfred Wegener Institute for Polar and Marine Research (AWI) and the French Polar Institute Paul-Émile Victor (IPEV)) station must be acknowledged for their support of both the NYTEFOX and ISLAS teams, especially Wilfried Ruhe. Additionally, we wish to thank the Norwegian Institute for Air Research (NILU) for the assistance rendered during our measurements at Zeppelin, especially Dorothea Schulze. We also want to express our gratitude to all individuals involved in the precipitation network collections, including: the UNIS staff, Vitaly Dekhtyarev, the staff at the Vervarslinga for Nord-Norge office, COMBLE field personnel (namely Juarez Viegas), Idar Barstad, and Alexandra Touzeau. We give hearty thanks to the technical staff at the Geophysical Institute, University of Bergen, who worked long and hard to help prepare equipment and handle logistics for the campaign, especially Anak Bhandari and Helge Bryhni. We would like to acknowledge the fine work of the data curators at PANGAEA for their expedited efforts to process the associated dataset. Finally, we wish to thank all those involved with the publishing of this manuscript, namely Marc Daniel Mallet for their editing efforts and we gratefully acknowledge the consideration and reviews from two anonymous referees, whose thoughts and feedback contributed to improving this work. This work has been funded by the European Research Council (Consolidator Grants ISLAS (project. 773245) and DarkMix (project. 724629)), as well as by the Research Council of Norway (project no. 291644) Svalbard Integrated Arctic Earth Observing System (SIOS) Knowledge Centre, operational phase.

References

Aemisegger, F., Sturm, P., Graf, P., Sodemann, H., Pfahl, S., Knohl, A., and Wernli, H.: Measuring variations of δ^{18}O and δ^{2}H in atmospheric water vapour using two commercial laser-based spectrometers: an instrument characterisation study, Atmospheric Measurement Techniques, 5, 1491–1511, https://doi.org/10.5194/amt-5-1491-2012, 2012.

Aemisegger, F., Trachsel, J., Sadowski, Y., Eichler, A., Lehning, M., Avak, S., and Schneebeli, M.: Fingerprints of Frontal Passages and Post-Depositional Effects in the Stable Water Isotope Signal of Seasonal Alpine Snow, Journal of Geophysical Research: Atmospheres, 127, e2022JD037 469, https://doi.org/https://doi.org/10.1029/2022JD037469, e2022JD037469 2022JD037469, 2022.

Bailey, A., Aemisegger, F., Villiger, L., Los, S. A., Reverdin, G., Meléndez, E. Q., Acquistapace, C., Baranowski, D. B., Böck, T., Bony, S., Bordsdorff, T., Coffman, D., Szoeke, S. P. D., Diekmann, C. J., Dütsch, M., Ertl, B., Galewsky, J., Henze, D., Makuch, P., Noone, D., Quinn, P. K., Rösch, M., Schneider, A., Schneider, M., Speich, S., Stevens, B., and Thompson, E. J.: Isotopic measurements in water vapor, precipitation, and seawater during EUREC4A, Earth System Science Data, 15, 465–495, https://doi.org/10.5194/essd-15-465-2023, 2023.

Barkan, E. and Luz, B.: Diffusivity fractionations of $H_2^{16}O/H_2^{17}O$ and $H_2^{16}O/H_2^{18}O$ in air and their implications for isotope hydrology, Rapid Communications in Mass Spectrometry, 21, 2999–3005, https://doi.org/10.1002/rcm.3180, 2007.

Berkelhammer, M., Noone, D. C., Steen-Larsen, H. C., Bailey, A., Cox, C. J., O'Neill, M. S., Schneider, D., Steffen, K., and White, J. W.: Surface-atmosphere decoupling limits accumulation at Summit, Greenland, Science Advances, 2, 1–10, https://doi.org/10.1126/sciadv.1501704, 2016.

Bonne, J. L., Masson-Delmotte, V., Cattani, O., Delmotte, M., Risi, C., Sodemann, H., and Steen-Larsen, H. C.: The isotopic composition of water vapour and precipitation in Ivittuut, southern Greenland, Atmospheric Chemistry and Physics, 14, 4419–4439, https://doi.org/10.5194/acp-14-4419-2014, 2014.

Brady, E., Stevenson, S., Bailey, D., Liu, Z., Noone, D., Nusbaumer, J., Otto-Bliesner, B. L., Tabor, C., Tomas, R., Wong, T., Zhang, J., and Zhu, J.: The Connected Isotopic Water Cycle in the Community Earth System Model Version 1, Journal of Advances in Modeling Earth Systems, 11, 2547–2566, https://doi.org/10.1029/2019MS001663, 2019.

Brunello, C., Gebhardt, F., Rinke, A., Dütsch, M., Bucci, S., Meyer, H., Mellat, M., and Werner, M.: Moisture Transformation in Warm Air Intrusions Into the Arctic: Process Attribution With Stable Water Isotopes, Geophysical Research Letters, 51, e2024GL111 013, https://doi.org/https://doi.org/10.1029/2024GL111013, e2024GL111013 2024GL111013, 2024.

Brunello, C. F., Meyer, H., Mellat, M., Casado, M., Bucci, S., Dütsch, M., and Werner, M.: Contrasting Seasonal Isotopic Signatures of Near-Surface Atmospheric Water Vapor in the Central Arctic During the MOSAiC Campaign, Journal of Geophysical Research: Atmospheres, 128, https://doi.org/10.1029/2022JD038400, 2023.

Cappa, C. D.: Isotopic fractionation of water during evaporation, Journal of Geophysical Research, 108, 4525, https://doi.org/10.1029/2003JD003597, 2003.

Casado, M., Landais, A., Picard, G., Arnaud, L., Dreossi, G., Stenni, B., and Prié, F.: Water Isotopic Signature of Surface Snow Metamorphism in Antarctica, Geophysical Research Letters, 48, e2021GL093 382, https://doi.org/https://doi.org/10.1029/2021GL093382, e2021GL093382 2021GL093382, 2021.

Craig, H.: Isotopic Variations in Meteoric Waters, Science, 133, 1702–1703, 1961.

Craig, H. and Gordon, L. I. L.: Deuterium and oxygen 18 variations in the ocean and the marine atmosphere, vol. 122, pp. 9–130, ISBN 1111111111, 1965.

Dahlke, S., Solbès, A., and Maturilli, M.: Cold Air Outbreaks in Fram Strait: Climatology, Trends, and Observations During an Extreme Season in 2020, Journal of Geophysical Research: Atmospheres, 127, 1–18, https://doi.org/10.1029/2021JD035741, 2022.

Dansgaard, W.: Stable isotopes in precipitation, Tellus, 16, 436–468, https://doi.org/10.3402/tellusa.v16i4.8993, 1964.

Divine, D. V., Sjolte, J., Isaksson, E., Meijer, H. A. J., van de Wal, R. S. W., Martma, T., Pohjola, V., Sturm, C., and Godtliebsen, F.: Modelling the regional climate and isotopic composition of Svalbard precipitation using REMO$_{iso}$: a comparison with available GNIP and ice core data, Hydrological Processes, 25, 3748–3759, https://doi.org/10.1002/hyp.8100, 2011.

Dunn, M. F. and Grice, G. K.: Warm Air Intrusion Into the Arctic, Monthly Weather Review, 103, 1137–1139, https://doi.org/10.1175/1520-0493(1975)103<1137:WAIITA>2.0.CO;2, 1975.

Ellehoj, M. D., Steen-Larsen, H. C., Johnsen, S. J., and Madsen, M. B.: Ice-vapor equilibrium fractionation factor of hydrogen and oxygen isotopes: Experimental investigations and implications for stable water isotope studies, Rapid Communications in Mass Spectrometry, 27, 2149–2158, https://doi.org/10.1002/rcm.6668, 2013.

Geerts, B., McFarquhar, G., Xue, L., Jensen, M., Kollias, P., Ovchinnikov, M., Shupe, M., DeMott, P., Wang, Y., Tjernstrom, M., Field, P., Abel, S., Spengler, T., Neggers, R., Crewell, S., Wendisch, M., and Lupkes, C.: Cold-Air Outbreaks in the Marine Boundary Layer Experiment (COMBLE) Field Campaign Report, Tech. rep., Oak Ridge National Lab. (ORNL), Oak Ridge, TN (United States), Oak Ridge National Laboratory (ORNL), Oak Ridge, TN (US), https://doi.org/10.2172/1763013, 2021.

Gerland, S., Pavlova, O., Divine, D., Negrel, J., Dahlke, S., Johansson, A. M., Maturilli, M., and Semmling, M.: Long-term monitoring of landfast sea ice extent and thickness in Kongsfjorden, and related applications (FastIce), https://sios-svalbard.org/sites/sios-svalbard.org/files/common/SESS%5f2019%5f06%5fFastIce.pdf, 2020.

Hu, J., Yan, Y., Yeung, L. Y., and Dee, S. G.: Sublimation Origin of Negative Deuterium Excess Observed in Snow and Ice Samples From McMurdo Dry Valleys and Allan Hills Blue Ice Areas, East Antarctica, Journal of Geophysical Research: Atmospheres, 127, e2021JD035 950, https://doi.org/https://doi.org/10.1029/2021JD035950, e2021JD035950 2021JD035950, 2022.

Hughes, A. G., Wahl, S., Jones, T. R., Zuhr, A., Hörhold, M., White, J. W. C., and Steen-Larsen, H. C.: The role of sublimation as a driver of climate signals in the water isotope content of surface snow: laboratory and field experimental results, The Cryosphere, 15, 4949–4974, https://doi.org/10.5194/tc-15-4949-2021, 2021.

Huss, J. M., Zeller, M. L., Pfister, L., Lapo, K. E., Littmann, D., Schneider, J., Schulz, A., and Thomas, C. K.: NYTEFOX - The NY-Ålesund TurbulencE Fiber Optic eXperiment investigating the Arctic boundary layer, Svalbard, Zenodo, https://doi.org/10.5281/zenodo.4756836, 2021.

IAEA: Reference sheet for international measurement standards, 2009.

Jocher, G., Karner, F., Ritter, C., Neuber, R., Dethloff, K., Obleitner, F., Reuder, J., and Foken, T.: The Near-Surface Small-Scale Spatial and Temporal Variability of Sensible and Latent Heat Exchange in the Svalbard Region: A Case Study, ISRN Meteorology, 2012, 1–14, https://doi.org/10.5402/2012/357925, 2012.

Jouzel, J. and Merlivat, L.: Deuterium and oxygen 18 in precipitation: Modeling of the isotopic effects during snow formation, Journal of Geophysical Research, 89, 11 749, https://doi.org/10.1029/JD089iD07p11749, 1984.

Kirbus, B., Schirmacher, I., Klingebiel, M., Schäfer, M., Ehrlich, A., Slättberg, N., Lucke, J., Moser, M., Müller, H., and Wendisch, M.: Thermodynamic and cloud evolution in a cold-air outbreak during HALO-(AC)^3: quasi-Lagrangian observations compared to the ERA5 and CARRA reanalyses, Atmospheric Chemistry and Physics, 24, 3883–3904, https://doi.org/10.5194/acp-24-3883-2024, 2024.

Klein, E. S., Cherry, J. E., Young, J., Noone, D., Leffler, A. J., and Welker, J. M.: Arctic cyclone water vapor isotopes support past sea ice retreat recorded in Greenland ice, Scientific Reports, 5, 1–9, https://doi.org/10.1038/srep10295, 2015.

Klein, E. S., Baltensperger, A. P., and Welker, J. M.: Complexity of Arctic Ocean water isotope (δ18O, δ2H) spatial and temporal patterns revealed with machine learning, Elementa: Science of the Anthropocene, 12, 00 127, https://doi.org/10.1525/elementa.2022.00127, 2024.

Kopec, B. G., Feng, X., Michel, F. A., and Posmentier, E. S.: Influence of sea ice on Arctic precipitation, Proceedings of the National Academy of Sciences, 113, 46–51, https://doi.org/10.1073/pnas.1504633113, 2016.

Leroy-Dos Santos, C., Masson-Delmotte, V., Casado, M., Fourré, E., Steen-Larsen, H. C., Maturilli, M., Orsi, A., Berchet, A., Cattani, O., Minster, B., Gherardi, J., and Landais, A.: A 4.5 Year-Long Record of Svalbard Water Vapor Isotopic Composition Documents Winter Air Mass Origin, Journal of Geophysical Research: Atmospheres, 125, 1–18, https://doi.org/10.1029/2020JD032681, 2020.

Maturilli, M.: Continuous meteorological observations at station Ny-Ålesund (2011-08 et seq), PANGAEA - Data Publisher for Earth & Environmental Science, https://doi.org/10.1594/pangaea.914979, 2020.

Maturilli, M., Herber, A., and König-Langlo, G.: Continuous meteorological observations at station Ny-Ålesund, 1993-08 to 2011-07, PANGAEA - Data Publisher for Earth & Environmental Science, https://doi.org/10.1594/pangaea.793046, 2013a.

Maturilli, M., Herber, A., and König-Langlo, G.: Climatology and time series of surface meteorology in Ny-Ålesund, Svalbard, Earth System Science Data, 5, 155–163, https://doi.org/10.5194/essd-5-155-2013, 2013b.

May, R. M., Goebbert, K. H., Thielen, J. E., Leeman, J. R., Camron, M. D., Bruick, Z., Bruning, E. C., Manser, R. P., Arms, S. C., and Marsh, P. T.: MetPy: A Meteorological Python Library for Data Analysis and Visualization, Bulletin of the American Meteorological Society, 103, E2273 – E2284, https://doi.org/10.1175/BAMS-D-21-0125.1, 2022.

Papritz, L. and Pfahl, S.: Importance of Latent Heating in Mesocyclones for the Decay of Cold Air Outbreaks: A Numerical Process Study from the Pacific Sector of the Southern Ocean, Monthly Weather Review, 144, 315–336, https://doi.org/10.1175/MWR-D-15-0268.1, 2016.

Papritz, L., Rouges, E., Aemisegger, F., and Wernli, H.: On the Thermodynamic Preconditioning of Arctic Air Masses and the Role of Tropopause Polar Vortices for Cold Air Outbreaks From Fram Strait, Journal of Geophysical Research: Atmospheres, 124, 11 033–11 050, https://doi.org/https://doi.org/10.1029/2019JD030570, 2019.

Pfahl, S., Wernli, H., and Yoshimura, K.: The isotopic composition of precipitation from a winter storm-a case study with the limited-area model COSMOiso, Atmospheric Chemistry and Physics, 12, 1629–1648, https://doi.org/10.5194/acp-12-1629-2012, 2012.

Pisso, I., Sollum, E., Grythe, H., Kristiansen, N. I., Cassiani, M., Eckhardt, S., Arnold, D., Morton, D., Thompson, R. L., Zwaaftink, C. D. G., Evangeliou, N., Sodemann, H., Haimberger, L., Henne, S., Brunner, D., Burkhart, J. F., Fouilloux, A., Brioude, J., Philipp, A., Seibert, P., and Stohl, A.: The Lagrangian particle dispersion model FLEXPART version 10.4, Geoscientific Model Development, 12, 4955–4997, https://doi.org/10.5194/gmd-12-4955-2019, 2019.

Schulz, A.: Untersuchung der Wechselwirkung synoptisch-skaliger mit orographisch bedingten Prozessen in der arktischen Grenzschicht über Spitzbergen, pp. 1–194, https://publishup.uni-potsdam.de/frontdoor/index/index/docId/40005, 2017.

Seidl, A. W., Sodemann, H., and Steen-Larsen, H. C.: A modular field system for near-surface, vertical profiling of the atmospheric composition in harsh environments using cavity ring-down spectroscopy, Atmospheric Measurement Techniques, 16, 769–790, https://doi.org/10.5194/amt-16-769-2023, 2023.

Seidl, A. W., Sodemann, H., Dekhtyareva, A., Huss, J. M., Thomas, C. K., Schulz, A., and Hermansen, O.: ISLAS2020: Calibrated stable water isotope measurements from Svalbard and coastal Norway during February and March 2020, https://doi.org/10.1594/PANGAEA.971241, 2024.

Shupe, M. D., Rex, M., Blomquist, B., Persson, P. O. G., Schmale, J., Uttal, T., Althausen, D., Angot, H., Archer, S., Bariteau, L., Beck, I., Bilberry, J., Bucci, S., Buck, C., Boyer, M., Brasseur, Z., Brooks, I. M., Calmer, R., Cassano, J., Castro, V., Chu, D., Costa, D., Cox, C. J.,

Creamean, J., Crewell, S., Dahlke, S., Damm, E., de Boer, G., Deckelmann, H., Dethloff, K., Dütsch, M., Ebell, K., Ehrlich, A., Ellis, J., Engelmann, R., Fong, A. A., Frey, M. M., Gallagher, M. R., Ganzeveld, L., Gradinger, R., Graeser, J., Greenamyer, V., Griesche, H., Griffiths, S., Hamilton, J., Heinemann, G., Helmig, D., Herber, A., Heuzé, C., Hofer, J., Houchens, T., Howard, D., Inoue, J., Jacobi, H.-W., Jaiser, R., Jokinen, T., Jourdan, O., Jozef, G., King, W., Kirchgaessner, A., Klingebiel, M., Krassovski, M., Krumpen, T., Lampert, A., Landing, W., Laurila, T., Lawrence, D., Lonardi, M., Loose, B., Lüpkes, C., Maahn, M., Macke, A., Maslowski, W., Marsay, C., Maturilli, M., Mech, M., Morris, S., Moser, M., Nicolaus, M., Ortega, P., Osborn, J., Pätzold, F., Perovich, D. K., Petäjä, T., Pilz, C., Pirazzini, R., Posman, K., Powers, H., Pratt, K. A., Preußer, A., Quéléver, L., Radenz, M., Rabe, B., Rinke, A., Sachs, T., Schulz, A., Siebert, H., Silva, T., Solomon, A., Sommerfeld, A., Spreen, G., Stephens, M., Stohl, A., Svensson, G., Uin, J., Viegas, J., Voigt, C., von der Gathen, P., Wehner, B., Welker, J. M., Wendisch, M., Werner, M., Xie, Z., and Yue, F.: Overview of the MOSAiC expedition: Atmosphere, Elem Sci Anth, 10, https://doi.org/10.1525/elementa.2021.00060, 2022.

Sodemann, H., Dekhtyareva, A., Seidl, A., and Johannessen, A.: COMBLE-Isotopic Links to Atmospheric Waters Sources (ISLAS) Snow Sampling 2020 Field Campaign Report, Tech. rep., Oak Ridge National Lab. (ORNL), Oak Ridge, TN (United States), Oak Ridge National Laboratory (ORNL), Oak Ridge, TN (US), https://doi.org/10.2172/1721761, 2020.

Sodemann, H., Dekhtyareva, A., Fernandez, A., Seidl, A., and Maccali, J.: A flexible device to produce a gas stream with a precisely controlled water vapour mixing ratio and isotope composition based on microdrop dispensing technology, Atmospheric Measurement Techniques, 16, 5181–5203, https://doi.org/10.5194/amt-16-5181-2023, 2023a.

Sodemann, H., Mørkved, P. T., and Wahl, S.: FLIIMP - a community software for the processing, calibration, and reporting of liquid water isotope measurements on cavity-ring down spectrometers, MethodsX, 11, 102 297, https://doi.org/10.1016/j.mex.2023.102297, 2023b.

Sodemann, H., Weng, Y., Touzeau, A., Jeansson, E., Thurnherr, I., Barrell, C., Renfrew, I. A., Semper, S., Våge, K., and Werner, M.: The Cumulative Effect of Wintertime Weather Systems on the Ocean Mixed-Layer Stable Isotope Composition in the Iceland and Greenland Seas, Journal of Geophysical Research: Atmospheres, 129, e2024JD041 138, https://doi.org/https://doi.org/10.1029/2024JD041138, e2024JD041138 2024JD041138, 2024.

Solomon, A., Shupe, M. D., Svensson, G., Barton, N. P., Batrak, Y., Bazile, E., Day, J. J., Doyle, J. D., Frank, H. P., Keeley, S., Remes, T., and Tolstykh, M.: The winter central Arctic surface energy budget: A model evaluation using observations from the MOSAiC campaign, Elementa: Science of the Anthropocene, 11, 00 104, https://doi.org/10.1525/elementa.2022.00104, 2023.

Steen-Larsen, H. C., Johnsen, S. J., Masson-Delmotte, V., Stenni, B., Risi, C., Sodemann, H., Balslev-Clausen, D., Blunier, T., Dahl-Jensen, D., Ellehøj, M. D., Falourd, S., Grindsted, A., Gkinis, V., Jouzel, J., Popp, T., Sheldon, S., Simonsen, S. B., Sjolte, J., Steffensen, J. P., Sperlich, P., Sveinbjörnsdóttir, A. E., Vinther, B. M., and White, J. W.: Continuous monitoring of summer surface water vapor isotopic composition above the Greenland Ice Sheet, Atmospheric Chemistry and Physics, 13, 4815–4828, https://doi.org/10.5194/acp-13-4815-2013, 2013.

Thomas, C. K., Huss, J. M., Abdoli, M., Huttarsch, T., and Schneider, J.: Solid-Phase Reference Baths for Fiber-Optic Distributed Sensing, Sensors, 22, 4244, https://doi.org/10.3390/s22114244, 2022.

Thurnherr, I. and Aemisegger, F.: Disentangling the impact of air–sea interaction and boundary layer cloud formation on stable water isotope signals in the warm sector of a Southern Ocean cyclone, Atmospheric Chemistry and Physics, 22, 10 353–10 373, https://doi.org/10.5194/acp-22-10353-2022, 2022.

Thurnherr, I., Hartmuth, K., Jansing, L., Gehring, J., Boettcher, M., Gorodetskaya, I., Werner, M., Wernli, H., and Aemisegger, F.: The role of air–sea fluxes for the water vapour isotope signals in the cold and warm sectors of extratropical cyclones over the Southern Ocean, Weather and Climate Dynamics, 2, 331–357, https://doi.org/10.5194/wcd-2-331-2021, 2021.

Valkonen, T., Stoll, P., Batrak, Y., Køltzow, M., Schneider, T. M., Stigter, E. E., Aashamar, O. B., Støylen, E., and Jonassen, M. O.: Evaluation of a sub-kilometre NWP system in an Arctic fjord-valley system in winter, Tellus A: Dynamic Meteorology and Oceanography, 72, 1–21, https://doi.org/10.1080/16000870.2020.1838181, 2020.

Wahl, S., Steen-Larsen, H. C., Reuder, J., and Hörhold, M.: Quantifying the Stable Water Isotopologue Exchange Between the Snow Surface and Lower Atmosphere by Direct Flux Measurements, Journal of Geophysical Research: Atmospheres, 126, 1–24, https://doi.org/10.1029/2020JD034400, 2021.

Wahl, S., Walter, B., Aemisegger, F., Bianchi, L., and Lehning, M.: Identifying airborne snow metamorphism with stable water isotopes, The Cryosphere, 18, 4493–4515, https://doi.org/10.5194/tc-18-4493-2024, 2024.

Weng, Y., Touzeau, A., and Sodemann, H.: Correcting the impact of the isotope composition on the mixing ratio dependency of water vapour isotope measurements with cavity ring-down spectrometers, Atmospheric Measurement Techniques, 13, 3167–3190, https://doi.org/10.5194/amt-13-3167-2020, 2020.

Wolff, M. A., Isaksen, K., Petersen-Øverleir, A., Ødemark, K., Reitan, T., and Brækkan, R.: Derivation of a new continuous adjustment function for correcting wind-induced loss of solid precipitation: results of a Norwegian field study, Hydrology and Earth System Sciences, 19, 951–967, https://doi.org/10.5194/hess-19-951-2015, 2015.

Zeller, M. L., Huss, J. M., Pfister, L., Lapo, K. E., Littmann, D., Schneider, J., Schulz, A., and Thomas, C. K.: The NY-Ålesund TurbulencE Fiber Optic eXperiment (NYTEFOX): investigating the Arctic boundary layer, Svalbard, Earth System Science Data, 13, 3439–3452, https://doi.org/10.5194/essd-13-3439-2021, 2021.